Solar position confounds the relationship between ecosystem function and vegetation indices derived from solar and photosynthetically active radiation fluxes.

Adrian V. Rocha[1], Rose Appel[1], M. Syndonia Bret-Harte[2], Eugenie Euskirchen[2], Verity Salmon[3], Gus Shaver[4]

[1]Department of Biological Sciences and the Environmental Change Initiative, Notre Dame, IN 46556, USA

[2]Institute of Arctic Biology, University of Alaska Fairbanks, Fairbanks, AK 99775, USA

[3]Environmental Sciences Division and Climate Change Science Institute, Oak Ridge National Laboratory, Oak Ridge, TN 37831, USA

[4]The Ecosystems Center, Marine Biological Laboratory, Woods Hole, MA 02543, USA

Submitted to: Agricultural and Forest Meteorology

Corresponding Author:
Adrian V. Rocha
University of Notre Dame
Department of Biological Sciences and the Environmental Change Initiative
100 Galvin Life Sciences
Notre Dame, IN 46556
Ph: 574-631-9438
Email: arocha1@nd.edu

Abstract:

Vegetation indices derived from solar and photosynthetically active radiation (PAR) sensors (i.e. radiation derived) have been under-utilized in inferring ecosystem function, despite measurement capability at hundreds of sites. This under-utilization may be attributed to reported mismatches among the seasonality of radiation- and satellite-derived vegetation indices and canopy photosynthesis; herein referred to as measurement biases. Here biases in radiation derived reflectance and vegetation indices were assessed using a decadal record of satellite and ground based spectroradiometer data, ecosystem phenology and CO_2 fluxes, and radiation derived vegetation indices (i.e. the Normalized Difference Vegetation Index [NDVI], the two band Enhanced Vegetation Index [EVI2]) from a high latitude tundra site (i.e. Imnaviat). At Imnaviat, we found poor correspondence between the three types of reflectance and vegetation indices, especially during the latter part of the growing season. Radiation derived vegetation indices resulted in incorrect estimates of phenological timing of up to a month and poor relationships with canopy photosynthesis (i.e. Gross Ecosystem Exchange (GEE)). These mismatches were attributed to solar position (i.e. solar zenith and azimuth angle) and a method, based on the diel visible and near-infrared albedo variation, was developed to improve the performance of the vegetation indices. The ability of radiation derived vegetation indices to infer GEE and phenological dates drastically improved once radiation derived vegetation indices were corrected for solar position associated biases at Imnaviat. Moreover, radiation derived vegetation indices became better aligned with MODerate resolution Imaging Spectroradiometer (MODIS) satellite estimates after solar position associated biases were corrected at Imnaviat and at 25 Fluxnet sites (~90 site years) across North America. Corrections developed here provide a way forward in

understanding daily ecosystem function or filling large gaps in eddy covariance data at a significant number of Fluxnet sites.

Keywords: Phenology, NDVI, EVI2, Solar Zenith, Gross Ecosystem Exchange, Arctic LTER

1.0 Introduction:

Vegetation indices, such as the Normalized Difference Vegetation Index (NDVI), have been used to infer ecosystem structure and function over the past half century (Rouse 1974). These indices utilize the low red reflectance -due to chlorophyll absorption-, and the high NIR reflectance -due to low absorption and high scattering- of green leaves to infer ecosystem function (e.g. leaf abundance, canopy physiology, and canopy phenology) (Gamon et al. 2010; Gamon et al. 2006). Historically, these indices were derived from satellite based reflectance; providing a proxy of ecosystem function at the global scale-albeit at low temporal resolution (e.g. monthly, bi-monthly). However, these indices also can be derived from commonly used up- and down-ward facing Photosynthetically Active Radiation (PAR) and solar radiation sensors (i.e. radiation derived); providing a low cost continuous measure of ecosystem function even when heavy cloud cover obscures satellite views of the surface (Huemmrich et al. 1999; Rocha and Shaver 2009; Wilson and Meyers 2007). Although radiation derived vegetation indices provide a powerful tool for understanding ecosystem function at sub-daily to annual timescales, a critical assessment of their uncertainties are surprisingly lacking.

Despite the wide use of PAR and solar radiation sensors across many eddy covariance sites, radiation derived vegetation indices have been under-utilized in inferring ecosystem function. Only a handful of studies have used radiation derived vegetation indices to infer ecosystem function, as compared to the thousands that have used satellite derived vegetation indices (Jenkins et al. 2007; Wohlfahrt et al. 2010; Wright and Rocha 2018). This imbalance may be due to the historical precedent of satellite data, or a lack of mechanistic understanding of measurement uncertainties in radiation derived indices. Radiation derived vegetation indices differ in magnitude and exhibit less seasonality than those derived from satellite data (Rocha and Shaver 2009). Jenkins et al. (2007) found that the slope of the relationship between radiation derived vegetation indices and canopy photosynthesis differed in the early and later part of the growing season. This contrasts with remote sensing work that models canopy photosynthesis from satellite derived vegetation indices with a single relationship across the season, and highlights a significant methodological knowledge gap (Sims et al. 2006; Sims et al. 2011; Xiao et al. 2005).

Although various hypotheses have been proposed to resolve the differences in radiation- and satellite- derived vegetation indices, the mechanisms are still debatable. The lack of correspondence between radiation- and satellite-derived vegetation indices have often been attributed to differences in the spatial scale of integration between the two measures or differences in sensor spectral resolution (Disney et al. 2004; Tittebrand 2009; Wang et al. 2004; Wang et al. 2012). Ground based radiation derived vegetation indices integrate a smaller area (i.e. ~100 x 100 m) than satellites such as the MODerate resolution Imaging Spectroradiometer (MODIS) (i.e. 100-1000 m) (Schmid 1997). Spatial mismatches are less likely to confound ground radiation- and satellite- derived reflectance and vegetation index comparisons in homogenous landscapes (Wittich and Kraft 2008). Radiation-derived vegetation indices also are very broad and integrate spectral information across the visible and infrared wavelengths, whereas satellite derived vegetation indices use more narrow spectral bands that focus on the red and NIR portions of the electromagnetic spectrum (Wittich and Kraft 2008). This spectral mismatch is more likely to influence the magnitude- but not the seasonality-of the vegetation indices. Although both these mechanisms are important at individual sites, they are unlikely to account for the large magnitude and consistency of radiation- and satellite-derived differences observed across many sites.

Sensor measurement biases have been largely overlooked when determining the causal mechanism behind differences in radiation- and satellite-derived vegetation indices (Balzarolo et al. 2011; Schaepman-Strub et al. 2006). Satellite sensors measure surface radiance and then corrects reflectance to minimize solar illumination and sensor view effects using a Bi-Directional Reflectance Function (BRDF) (Schaepman-Strub et al. 2006). The BRDF corrects for solar illumination effects from solar position to compare reflectance at the same view angle-typically defined at nadir. Such corrections are not made for radiation derived vegetation indices (Balzarolo et al. 2011; Huemmrich et al. 1999; Wilson and Meyers 2007). Although the radiation sensors are located above the canopy, these sensors integrate radiation from the entire hemisphere. Despite this hemispherical field of view, shortwave albedo has been shown to be sensitive to illumination angle (i.e. solar zenith and azimuth angles), which changes over the course of a day and year (Huemmrich et al. 1999). For example, broadband albedo measured with pyranometers have been shown to be dependent on solar zenith angle and illumination intensity for surfaces with high reflectivity such as snow (Carroll and Fitch 1981; Kriebel 1979; Wang et al. 2005; Wang and Zender 2010; Yang et al. 2008). However, little has been done to understand or correct the impact of illumination angle effects on radiation derived vegetation indices.

Here we assessed the ability of PAR and solar radiation derived reflectance proxies and vegetation indices to replicate MODIS satellite derived reflectance and vegetation indices; herein referred to as measurement biases. We also assessed the ability of PAR and solar radiation derived vegetation indices to infer ecosystem function (i.e. plant phenology and CO_2 fluxes). We focus on two commonly used vegetation indices: NDVI and EVI2 (Rocha and Shaver 2009). NDVI has more of a historical precedent in inferring ecosystem function, but EVI2 may provide a better proxy of ecosystem function due to its insensitivity to non-vegetated background reflectance (Jiang et al. 2008). Past remote sensing work has demonstrated the impact of solar position in influencing reflectance and vegetation indices, but lacked biological data to demonstrate the implications of ignoring such biases for inferring ecosystem function (Bhandari et al. 2011; Huete 1987; Ma et al. 2019; Middleton 1992). We hypothesized that solar position will lead to systematic biases in radiation derived vegetation indices that prevent these indices from correctly inferring vegetation phenology and seasonality in canopy photosynthesis at Imnaviat. We tested this hypothesis with a decadal record of PAR and solar radiation fluxes, MODIS, and ground based spectral radiometer measurements at a high latitude tundra site (Imnaviat), and further corroborated the patterns observed at Imnaviat with a synthesis of Fluxnet datasets. Imnaviat was chosen because of its landscape homogeneity, its rich long term ecological dataset (i.e. long term CO_2 fluxes and plant phenology), as well as its high latitude location with a frequently high solar zenith angle. The attributes of these data provide an ideal opportunity to determine the major sources of measurement biases leading to the discrepancy between satellite- and radiation-derived vegetation indices, and measures of seasonality in ecosystem function.

2.0 Methods

2.1 Site Description, Instrumentation, and Available Data

This study was conducted on a west-facing hillslope within the Imnaviat Creek watershed on the North Slope of Alaska, USA (68.61° N; 149.31° W). Vegetation at the site was characteristic of moist acidic tussock tundra with tussock cottongrass [*Eriophorum vaginatum*], dwarf birch [*Betula nana*], labrador tea [*Rhododendron tomentosum*], sphagnum moss [*Sphagnum spp.*], and scattered lichens covering the landscape (Euskirchen et al. 2012). The mean annual temperature at the site was -7 °C and the mean annual precipitation was 318 mm, with 40% occurring as rain and 60% as snow. Mean growing season (June-August) temperature was 6 °C, while mean non-growing season temperature was -11 °C.

In July of 2008, Imnaviat was instrumented with three (1 upward and two downward) CMP3 pyranometers that measured shortwave solar radiation (SW: units: W m^{-2}) [CMP3; Kipp and Zonen], three PAR sensors that measured Photosynthetically Active Radiation (PAR: units: µmol m^{-2} s^{-1}) [LI-190SA; Li-Cor, Lincoln NB], two downward looking surface temperature radiometers [IRT Infrared Thermometer; Apogee Instruments], a HMP temperature and humidity sensor [HMP45C-L; Campbell Scientific], and two TCAV soil temperature sensors [TCAV-L; Campbell Scientific]. Meteorological sensors were mounted at a height of 2.5 meters. Radiation sensors were well maintained, frequently leveled, and sent for factory calibration every 2-3 years during the measurement period. The radiation tower ran nearly continuously from July 2008-2018, and was powered by a battery bank connected to two solar panels, which were situated away from the direct field of view of the sensors.

The radiation tower was located ~300 m away from three Arctic Observatory Network (AON) flux towers located along the same west facing hillslope gradient (Euskirchen et al. 2012). The flux towers measured the Net Ecosystem Exchange of CO_2 (NEE) via the eddy covariance method, and a suite of meteorological variables including incoming and outgoing PAR and solar radiation, air temperature, humidity, wind speed, soil moisture, soil temperature, and snow depth (Baldocchi 2003). We analyzed the mean seasonal cycle of the daily Gross Ecosystem Exchange (GEE) at the mid-slope Moist Acidic Tundra (MAT) site from 2008-2018 to determine the relationship between vegetation indices and the seasonality of photosynthesis. The mid-slope MAT flux tower was chosen because of its similar vegetation composition, slope position, and NDVI seasonality to the nearby radiation tower [MAT Flux Tower NDVI vs. Imnaviat Radiation Tower NDVI R^2: 0.97; Slope: 1.01; Mean Absolute Error (MAE): 0.01]. AON data were obtained online at http://aon.iab.uaf.edu.

NEE flux partitioning was described in detail in Euskirchen et al. (2012, 2017), and followed standard Fluxnet protocols for partitioning NEE into canopy photosynthesis (Gross Ecosystem Exchange: GEE) and ecosystem respiration (ER). Briefly, NEE flux partitioning was accomplished by fitting a Q10 air temperature response function to well mixed (u-star> 0.10 s m^{-1}) NEE's that occurred during low light conditions (PAR< 50 µmol m^{-2} s^{-1}) (Ueyama et al. 2013; Euskirchen et al. 2017)). The basal respiration and Q10 parameters of the exponential model were determined through least squares fitting with "low light" NEE and air temperature data from a 30 day daily moving window. This empirically derived Q10 air temperature response function was used to estimate half hourly ER. Half hourly GEE was inferred from NEE by subtracting ER from NEE (GEE=NEE-ER), and temporally scaled up with daily summations.

2.2 Ground based Spectral Reflectance Measurements

Ground based reflectance was measured within the footprint of the Imnaviat radiation tower using three different spectroradiometers over the years. Spectral reflectance was measured with a Unispec (UniSpec-SC, PP-Systems, Amesbury, MA; Spectral Range: 300-1200 nm at 2 nm resolution) from 2008-2009, a dual channel Unispec (Unispec-DC, PP-Systems, Amesbury, MA; Spectral Range: 300-1200 nm at 2 nm resolution) from 2010-2012, and a FieldSpec 4 (Analytical Spectral Devices (ASD); Malvern Panalytical Ltd; United Kingdom; Spectral Range: 200-2400 nm at 2 nm resolution) from 2013-2018. Four ~100 m transects separated by ~30 m were established on the North and South side of the radiation tower forming a 200x120m grid within the tower footprint. Spectral reflectance was measured during midday hours (11:00 am-2:00 pm AST) every ~3 meters along each of the four 100 m transects either weekly, bi-monthly, or monthly during the growing season (June-August) of each year (n=240 scans per sampling date). A total of 62 sampling campaigns were undertaken from July 2008 to August 2018 with each campaign taking ~1 hour to accomplish.

Surface reflectance measurements followed standard procedures described in the spectroradiometer user manuals. Prior to measurements, each instrument was allowed a 15-20 minute warm up period. A freshly cleaned white Spectralon® diffuse reflectance panel

(Labsphere; North Sutton, NH) was used as a reflectance standard to convert spectroradiometer derived radiance into surface reflectance. Dark current measurements were taken by closing the detector "door", which prevented light from hitting the detectors and minimized measurement artifacts from background electrical instrument noise. Optimal measurement integration times were dependent on illumination conditions and were automatically determined by each sensor. White panel, dark current, and optimal measurement integration time measurements were taken frequently (i.e. every 3-5 minutes depending on sky conditions) to ensure high quality reflectance data. After each sampling campaign, surface reflectance data were quality checked for anomalous spectra (i.e. spectra that were >3 standard deviations from the mean) and averaged across all scans. These spectra were used to calculate NDVI and EVI2 using Equations [2] and [3] below and spectrally averaged MODIS wavelength definitions for red- (average of 620-670 nm) and NIR- reflectance (average of 841-876 nm) (Schaaf et al. 2002). We also spectrally averaged all wavelengths to calculate total and visible reflectance to derive a broad band visible, NIR (using equation 1), NDVI and EVI2 based on ASD spectroradiometer data. ASD averaged total reflectance was within 10% of the shortwave albedo, while ASD averaged visible reflectance was within 5% of PAR albedo measured by radiation sensors at Imnaviat.

2.3 Ground based Phenology

Individual plant species phenologies were measured from 2008-2018 in moist acidic tundra at the Toolik Lake Arctic Long Term Ecological Research (LTER) station. Toolik field station was situated ~7 km away and experienced similar weather to Imnaviat. A variety of phenological events (i.e. first snow free, first visible leaf, first leaf drop, first color change, and last leaf drop) were measured in several plots around Toolik lake in each year for the dominant MAT species (i.e. *Andromeda polifolia, Betula nana, Carex bigelowii, Cassiope tetragona, Empetrum nigrum, Eriophorum vaginatum, Ledum palustre, Polygonum bistorta, Rubus chamaemorus, Salix pulchra, Vaccinium uliginosum, Vaccinium vitis-idaea*). These phenological data were used to validate satellite- and radiation- derived NDVI and EVI2 estimates of the start-, end-, and length- of the growing season. The average of the first visible leaf for all species served as a proxy for the start of the growing season, whereas the maximum last leaf color change served as a proxy for the end of the growing season.

2.4 Radiation derived Vegetation Indices

The radiation tower at Imnaviat measured surface albedo in the visible (400-700 nm) and total shortwave wavelengths (300-2400 nm) of light. These albedo measures served as a proxy for red and near infrared reflectance (Rocha and Shaver 2009). Visible (α_V) albedo was calculated as the ratio between reflected ($_r$) and incoming ($_i$) PAR $\alpha_V = PAR_r/PAR_i$, while total albedo (α_T) was calculated as the ratio between reflected and incoming shortwave radiation [SW_r & SW_i, respectively] $\alpha_T = SW_r/SW_i$. α_V was used as a proxy for red reflectance, while both α_V and α_T were used in Equation 1 as a proxy for NIR reflectance (α_N) (Jenkins et al. 2007).

$$\alpha_N = W * \alpha_T - \alpha_V \qquad \textbf{Equation [1]}$$

W in Equation 1 equaled 2 for all vegetation types, and represented a weighting term to separate α_N from α_V and α_T. Derivations of red and near infrared reflectance from ground based radiometers represented broadband definitions of narrowband quantities. α_N included dynamics in the near- and short-wave infrared region of the reflectance spectrum, while α_V included dynamics in the red, blue and green regions of the reflectance spectrum. Other ground radiometer derivations of α_N utilize similar assumptions (see Huemmrich et al., 1999 & Wilson and Meyers, 2007). We used Jenkins et al. (2007) derivation because of its parsimony and its high correlation with other α_N derivations (Jenkins vs. Huemmrich R^2 [Mean Absolute Error: MAE]: 0.91 [0.015]/ MAE Jenkins vs. Wilson & Meyers R^2 [MAE]: 0.99 [0.014]) for the sites used in this study. We also found that the conclusions from our analyses were independent of the different formulations of α_N.

We focused our analyses on the active growing season during snow-free periods. Data influenced by snow covered ground were identified with an albedo threshold of >0.3 (i.e. vegetation albedo <0.25 at all sites) and removed from the half hourly radiation datasets. Incoming and reflected radiation were averaged over the course of a day (i.e. n=48 for each value) to minimize diel solar zenith effects (Huemmrich et al. 1999; Rocha and Shaver 2009; Wilson and Meyers 2007). Sensor drift and snow and dirt accumulation on the sensors were identified as periods where PAR_i/SW_i fell beyond or below the mean plus or minus 2 standard deviations and subsequently removed. The final "cleaned" dataset contained daily ground radiometer values that were compared with MODIS reflectance and vegetation indices.

NDVI and EVI2 were calculated from radiation-, spectroradiometer- and MODIS-derived measures of near infrared (α_N) and red reflectance (α_R) with Equations [2] and [3] (Jiang et al. 2008).

$$NDVI = \frac{\alpha_N - \alpha_R}{\alpha_N + \alpha_R}$$ **Equation [2]**

$$EVI2 = 2.5\frac{\alpha_N - \alpha_R}{\alpha_N + 2.4\alpha_R + 1}$$ **Equation [3]**

2.5 Fluxnet Data Synthesis

We conducted a broader survey of ground based radiation derived vegetation indices with Fluxnet data to determine whether biases observed at the Imnaviat site were consistent across other sites (Table 1). Data from the Fluxnet network consisted of 25 sites and 90 site years of half hourly incoming ($_i$) and reflected ($_r$) PAR and shortwave data (Table 1). 12% of the sites were from crops, 8% were from deciduous forests, 25% were from evergreen forests, 28% were from grasslands, 20% were from arctic tundra, and 8% were from a shrub and grassland mix. Sites had a minimum of two years of data with a maximum of 6 years at 2 sites, and an average of 3.5 years for the entire dataset. PAR within the 400-700 nm spectral region was measured with a LI190 quantum sensor (LI-COR Inc., Lincoln, Nebraska) at 85% of the sites, while the remaining sites used either an Apogee quantum sensor (Apogee Instruments, Logan, Utah) or BF3 sunshine sensor (Dynamax, Houston Texas). Shortwave radiation (SW) within the 300-2800 nm spectral region was measured with a CM3 (Kipp & Zonen, Bohemia, NY) at 90% of the sites, while the remaining sites used an Apogee pyranometer (Apogee Instruments, Logan, Utah) or LI200 pyranometer (LI-COR Inc., Lincoln, Nebraska). Data were aligned with MODIS satellite data (see section 2.7) through 16- day averages that were centered on the MODIS composite date.

2.6 Testing and Correcting for Solar Position Biases

We corrected solar position biases using diel relationships between solar position and albedo throughout the season. Diel NIR and visible albedo variability can be more than twice as large as observed over the course of a season (Huemmrich 1999). These large diel visible and NIR albedo variations cannot be representing changes in canopy leaf area, that are often related to vegetation indices, because LAI changes over much longer time scales than a day (i.e. days to weeks)(Stoy 2013). Rather, this large diel variation arises from the anisotropic properties of surface reflectance (i.e. the bidirectional reflectance distribution function) and possibly other sensor issues, such as a sensors' cosine response function (Huete 1987; Middleton 1992; Rahman et al. 1993).

Here we used the diel variation in albedo and solar position to empirically derive a correction factor to apply over the course of the season. We removed vegetation phenology impacts on the seasonal variability by dividing each daily averaged visible and NIR albedo into each half hourly visible and NIR albedo value to focus solely on sub-daily variations associated with solar position (Equation 4). These ratios provided 48 half hourly correction factors for each day and albedo that can be related to sub-daily solar position changes. When multiplied with each half hourly NIR or visible albedo, the correction factor scaled these values down to represent a consistent daily average for all 48 half hourly periods. These constant daily NIR and visible albedos were consistent with the fact that canopy leaf area does not significantly change on sub-daily timescales.

$$\alpha_{Cor} = \frac{Daily\ Value}{Half\ Hourly\ Value} = \frac{\alpha_d}{\alpha_h}$$ **Equation [4]**

α_{Cor} was calculated and three dimensional bin averaging on half hourly solar zenith, solar azimuth, and α_{Cor} helped establish the empirical relationship among the three variables. Because α_{Cor} was derived across the season and years, we used bin averaging to further smooth the α_{Cor} response function in relation to solar zenith and azimuth. We found that twenty-five equal range sized bins were sufficient enough to smooth the remaining variability associated with seasonal changes in solar zenith and azimuth angle and random noise in the albedo measurements. Machine learning methods with a squared exponential Gaussian process regression model along with the binned half hourly α_V and α_N were used to derive the empirical correction factor equations for each albedo measure (i.e. α_V and α_N) as a function of solar position. Empirical correction factors for each day were predicted from the daily averaged solar zenith and azimuth angle, and then multiplied by the daily averaged visible and NIR albedo to produce a solar position corrected α_V and α_N. NDVI and EVI2 were then recalculated using the solar position corrected α_V and α_N with Equations 2 and 3. Solar position was calculated for each site and half hour using the site latitude and longitude and time of year (Myers 2017). Analyses were accomplished with Matlab's Regression Learner application (MATLAB 2019b; Mathworks Inc. Natick, MA).

2.7 MODIS Data

We compared MODIS reflectance and vegetation indices to radiation derived proxies and measures. MODIS version 4 data were extracted from a 0.25 km^2 area centered at each tower location (http://daac.ornl.gov) (ORNL DAAC 2018). For Imnaviat, we used daily Nadir BRDF-

Adjusted reflectance (MCD43A4) and extracted data at various spatial scales (i.e. 0.25, 6.25, 20.25, 210.25, and 420.25 km^2) to determine the impact of spatial aggregation on the comparison between ground and satellite based data (Shuai et al. 2013). For the Fluxnet Data Synthesis, we used Nadir-BRDF adjusted 500 m resolution surface reflectance (MODIS NBAR; MCD43A) from seven spectral bands (Schaaf et al. 2002). We also used the seven MODIS spectral bands along with empirical equations from Liang (2000) to calculate a total and visible albedo that were used to derive broadband vegetation indices following Equations 1-3. MCD43A reflectance was reported every eight days, derived from both Terra and Aqua platforms, and adjusted to local solar noon with a BRDF calculated over a 16-day interval. Data with >80% of pixels passing quality control were used in the analyses. Only growing season MODIS data, as defined by ground based snowless terrestrial albedo values, were used in the analyses.

2.8 Phenology Model

The start, end, and length of the growing season was determined with a phenology model fit to the observed seasonal cycle of MODIS- and radiation- derived NDVI and EVI2 in each year at Imnaviat. The phenology model was a double-logistic function that predicted each vegetation index based on the day of year (t) (Beck et al. 2006; Fisher et al. 2006; Fisher et al. 2007) (Equation 5):

$$v(t) = v_{min} + v_{amp}\left(\frac{1}{1+e^{m_1-n_1 t}} - \frac{1}{1+e^{m_2-n_2 t}}\right) \qquad \textbf{Equation [5]}$$

The model was fit by minimizing the sum of squared residuals between model predictions and observed values. The fitted parameters of the model were v_{min} and v_{amp}, m_1, n_1, m_2, and n_2. v_{min}

and v_{amp} were related to the minimum and amplitude values of the spectral index, respectively. The parameters in the two exponents determined the seasonality with m_1 and n_1 related to the rate and timing of green-up, and m_2 and n_2 related to the rate and timing of senescence. The start of the growing season was given by $t = m_1/n_1$, the end of the growing season was given by $t = m_2/n_2$, and the length of the growing season was determined by the difference between the start and end of the growing season.

2.9 Statistical Analyses:

Statistical analyses included least squares linear regression to determine the relationship between two variables, and Mean Absolute Error (MAE) to determine the prediction error of a model or the error associated with the comparison of a set of similar observations (Ramsey 2013). Statistical significance was determined at the 95% confidence level.

3. Results

3.1 Assessing Spatial Aggregation Biases

The scale of spatial integration had little impact on the comparison between tower and MODIS based vegetation indices indicating landscape coherence in phenology within the region surrounding Imnaviat (Figure 1). Here we minimized spectral definition differences among sensors by comparing spectroradiometer- and MODIS- derived reflectance's and vegetation indices. Spectroradiometer derived NDVI explained 70% of the variability in MODIS derived NDVI, whereas spectroradiometer derived EVI2 explained 60% of the variability in MODIS derived EVI2. The MAE increased slightly from 6% of NDVI at the ecosystem/watershed level

(0-10 km^2) to 7% of NDVI at the regional scale (>300 km^2). EVI2 exhibited greater sensitivity to spatial integration with MAEs increasing from 14% of EVI2 at the ecosystem/watershed scale to 20% of EVI2 at the regional scale.

3.2 MODIS- vs. radiation-derived reflectance and indices comparison

In general, spectroradiometer- and MODIS- derived reflectances and vegetation indices were more related to each other than those derived from radiation fluxes at Imnaviat (Table 2). Vegetation indices yielded higher correlations among measurement types than did red and NIR reflectance. For example, reflectance R^2's ranged from 0.17-0.22 for NIR and red reflectance, while vegetation index R^2's ranged from 0.34 to 0.67. Correlations among radiation-, spectroradiometer-, and MODIS-derived measures were typically higher for EVI2 than for NDVI. The poor relationships between radiation- and MODIS/spectroradiometer- derived vegetation indices were largely attributed to differences in seasonality among the MODIS/spectroradiometer- and radiation- derived measures.

Seasonality differed among radiation-, spectroradiometer-, and MODIS derived- reflectance and vegetation indices at Imnaviat (Figure 2). Correspondence among the three measures was greatest for red reflectance and smallest for NIR, NDVI, and EVI2. Red reflectance demonstrated similar seasonality among the measures with higher reflectance in the shoulder seasons and minimum values during the peak of the growing season. In contrast, NIR reflectance, NDVI, and EVI2 were low at the start of the growing season, reached a maximum during peak growing season, and then declined to a minimum at the end of the growing season. All three measures of NIR, NDVI and EVI2 exhibited similar seasonality up until the peak of the growing season, but differed towards the end of the growing season. Radiation-derived NIR reflectance and vegetation indices were larger than MODIS and spectroradiometer- derived quantities towards the latter part of the growing season. Consequently, differences between MODIS and spectroradiometer- and radiation-derived NIR, NDVI, and EVI2 exhibited strong seasonality with the largest mismatch towards the second half of the growing season.

3.3 Assessing Sensor Biases

Seasonal differences between MODIS- and radiation- derived indices observed in Figure 2 were correlated with solar zenith angle at Imnaviat (Figure 3). Larger solar zenith angles produced larger differences between MODIS- and radiation- derived NIR, NDVI, and EVI2, but had no impact on differences between MODIS- and radiation- derived red reflectance. Solar zenith angle explained 41% of the variability in NIR reflectance biases, 28% of the variability in NDVI biases, and 45% of the variability in EVI2 biases. This represented a bias of 0.004 per 1° change in zenith angle for NIR reflectance, and a bias of 0.006 per 1° change in zenith angle for NDVI and EVI2.

The relationship between measurement bias and solar zenith angle at Imnaviat were consistent across Fluxnet sites located in vastly different biomes (Figure 4). However, in contrast to the observed solar zenith dependent measurement biases at the Imnaviat site, there was a statistically significant measurement bias dependence on solar zenith angle at some of the Fluxnet sites for red reflectance. For the Fluxnet dataset, MODIS and radiation derived NIR differences positively scaled with solar zenith angle and all biomes exhibited similar slopes that ranged from 0.002 to 0.003 per 1° change in zenith angle. The solar zenith dependent biases in NIR and red reflectance carried over to NDVI and EVI2, but sometimes canceled each other out. This cancelling out effect was more predominant for NDVI than for EVI2. For example, NDVI biases were unrelated to solar zenith angle for evergreens and grass shrublands, whereas solar zenith angle was correlated with EVI2 biases in all biomes. The bias sensitivity to solar zenith angle ranged from 0.001 to 0.005- for NDVI, and from 0.003 to 0.005- per 1^{o} change in zenith angle for EVI2.

3.4 Assessing Bandwidth Biases

We used the full range spectroradiometer ASD data (300-2400 nm) to determine whether the measurement bias dependence on solar position was attributed to broadband versus narrowband definitions of red and near infrared reflectance used by the radiation sensors (Figure 5). Correlations between solar zenith angle and the difference between broadband and narrowband (i.e. Bandwidth Biases) definitions for red (p-value: 0.94), NDVI (p-value: 0.21), and EVI2 (p-value: 0.06) were not statistically significant. Bandwidth biases were marginally significant and related to solar zenith angle for NIR (p-value: 0.05), but were opposite in sign to the expected relationships observed in Figures 3 & 4. Moreover, solar zenith angle only explained 10% of the variation in bandwidth biases, as opposed to the 67% of the variation in radiation tower and MODIS differences explained by zenith angle in Figure 3.

Similar results were found across the Fluxnet sites using MODIS data and differencing broad- and narrow- band vegetation indices (Figure 1S; Table 1S). Although many relationships were statistically significant, solar zenith angle only explained <10% of the variation in bandwidth biases for NDVI, and <11% of the variation in bandwidth biases for EVI2 across all Fluxnets sites on average (Supplementary Figure 1). Moreover, the bandwidth bias sensitivity to solar zenith angle was sometimes the opposite sign of the expected positive relationships in Figures 3 and 4 and were on average one to two orders of magnitude lower than that observed for tower and MODIS differences for red, NIR, NDVI, and EVI2 (Supplementary Table 1).

3.5 Correcting Solar Position Biases

Diel variability in solar position affected radiation derived visible and NIR albedos that were used as red and NIR reflectance at Imnaviat (Figure 6). Over the growing season, daily averaged solar zenith angle changed by 19°, while daily averaged solar azimuth angle changed by 7° (Figure 6 inset). Visible and NIR albedo were more sensitive to solar zenith- than azimuth- angles as illustrated by the small scatter in Figure 6. NIR albedo was more sensitive to solar zenith angle than visible albedo and was almost two times higher than its expected value at an 80° zenith angle. Consequently, the correction factor for NIR albedo declined markedly above 70° from 0.85 to 0.59, whereas the correction factor for visible albedo changed by <1% above 70° solar zenith angle.

Correcting solar position biases using the machine learning approach described in section 2.6 improved the agreement between MODIS- and radiation- derived red and NIR reflectance, NDVI, and EVI2 at Imnaviat (Figure 7). After correcting for the dependence of measurement biases on solar position, MAE decreased and R^2 increased between MODIS- and radiation- derived reflectance and vegetation indices (Table 3; Figure 7). An exception to this occurred for MODIS red reflectance, where the R^2 and MAE did not significantly change after correction due to its low sensitivity to solar position. MAE decreased by 40% for NDVI and EVI2, and by 33% for NIR reflectance after applying the correction factor for seasonal changes in solar position.

Correcting solar position biases using the machine learning approach also improved the agreement between MODIS- and radiation-derived NDVI and EVI2 across the Fluxnet sites (Figure 8). Correcting for measurement biases introduced by solar position reduced the MAE between MODIS- and radiation- derived NDVI and EVI by 5% to 77%. Grasslands and tundra experienced the largest decrease in MAE, while crops experienced the smallest decreases in MAE once the impact of solar position on radiation derived albedo and vegetation indices were corrected. There was quite a bit of variability in the improved correspondence between MODIS- and radiation-derived vegetation indices among sites. However, it was difficult, if not impossible, to attribute this variability to underlying environmental, biophysical or site specific factors without additional site and sensor specific information. Regardless, correcting biases in vegetation indices for solar position improved the correspondence between MODIS- and radiation- derived vegetation indices at 85% of the sites investigated.

3.6 Implications for Inferring Ecosystem Function with radiation derived NDVI and EVI2

Biases associated with solar position confounded the ecophysiological interpretation of radiation derived NDVI and EVI2 at Imnaviat (Figure 9). Uncorrected radiation derived vegetation indices exhibited hysteretic relationships with GEE with different sensitivities-as measured by the slope of the line- in the first and second half of the growing season. GEE was lower for the same value of NDVI/EVI2 in the first part of the growing season, and higher for the same value of NDVI/EVI2 in the second part of the growing season. The relationship between NDVI/EVI2 became more linearized with a single relationship throughout the growing season once vegetation indices were corrected for their solar position dependence (Figure 9 solid line). Uncorrected NDVI explained 37% of the variability in GEE, whereas solar position corrected NDVI explained 85% of the variability in GEE. Similar patterns were found for EVI2. Uncorrected EVI2 explained 37% of the variability in GEE, whereas solar position corrected EVI2 explained 89% of the variability in GEE.

Solar position also confounded the determination of the start, end, and length of the growing season at Imnaviat (Figure 10). On average, correcting radiation derived vegetation indices for solar position decreased the MAE between leaf level measures of phenology up to ~10 days. Differences between corrected and uncorrected NDVI/EVI2 derived phenologies were greatest for the length of the growing season due to compounding errors associated with the start and end of the growing season estimates. Uncorrected NDVI/EVI2 demonstrated reduced skill at determining the end of the growing season relative to the start; a finding that is consistent with trends observed in Figure 2. Solar position corrected radiation derived NDVI/EVI2 performed similarly to-or in some cases-better than MODIS in predicting the start and end of the growing season, especially for EVI2. For example, solar position corrected radiation derived EVI2 performed better than MODIS EVI2 in predicting the start and length of the growing season. When MODIS- and radiation- derived phenological predictions were combined, NDVI outperformed EVI2 by 5 days for the start of the growing season and 7 days for the length of the growing season, whereas EVI2 outperformed NDVI by 1 day for the end of the growing season.

4.0 Discussion:

Solar position introduced significant bias on PAR and solar radiation derived vegetation indices, especially during the latter part of the growing season. These errors were largely independent of broad- to narrow-band definitions (Figures 5 & 1S; Table 1S), and sensor spatial aggregation errors associated with landscape heterogeneity (Figure 1). The effect of satellite spatial aggregation errors was minimized by focusing on a relatively homogenous site (i.e. Imnaviat), and were much smaller than that observed for measurement biases [i.e. <0.02 change in vegetation index MAE from 0-400 km^2 (Figure 1) compared to ~0.05 MAE for tower and MODIS vegetation comparisons (Table 2)] (Wang et al. 2012). Measurement biases also were universal and occurred across a wide variety of latitudes, biomes, and sites indicating a persistent error that cannot be explained by individual site specific conditions (Figures 3,4,7,8). These measurement biases accounted for some of the limitations and issues highlighted in previous work with radiation derived vegetation indices (Jenkins et al. 2007; Rocha and Shaver 2009; Wang et al. 2004; Wittich and Kraft 2008). To our knowledge, this is the first paper, since Huemmrich et al.'s (1999) seminal work, to develop a methodology using the diel variation in albedo to correct for these biases and improve the performance of these indices in inferring ecosystem function.

Historically, solar position biases on radiation- derived albedo and vegetation indices were assumed to be negligible over the course of a season, despite known diel variation (Huemmrich et al. 1999). This incorrect assumption was likely due to data limitations from looking at a single site over a short time period, the exclusion of solar azimuthal effects, and a lack of multi-sensor comparisons. Unlike past work, our conclusions were supported by multiple independent physical and ecological observations. First, solar position corrections improved correspondence between satellite- and radiation- derived vegetation indices at Imnaviat and Fluxnet sites (Figures 7 and 8; Table 3). Second, solar position corrections improved the ability of radiation derived vegetation indices in capturing phenological timing and C fluxes (Figures 9 and 10). It is clear that our use of combining long time series data obtained from different sensors and scales was essential in validating and assessing measurement biases in radiation derived vegetation indices. Our results also demonstrated that, in some cases, solar position associated NIR and visible biases canceled each other out in the calculation of the vegetation index. This cancelation effect may explain the discrepancy between this study and past work at single sites that assumed negligible solar position biases.

Addressing solar position biases in visible and NIR albedo are important because these biases resulted in poor relationships with MODIS data and poor inferences of ecosystem function. Without correcting for solar position, measurement biases reduced the explained variation in canopy photosynthesis and increased estimation error of the start, end, and length of the growing season (Figures 9,10). Radiation derived vegetation indices also exhibited less seasonality than MODIS, which was consistent with previous work with higher than expected NIR and vegetation indices towards the latter part of the growing season (Rocha and Shaver 2009; Wittich and Kraft 2008). These unique attributes of radiation derived vegetation indices have been previously reported, but often incorrectly attributed to bandwidth biases rather than solar position (Rocha and Shaver 2009; Jenkins et al. 2007; Wang et al. 2004). Broadband derivations of red and NIR reflectance incorporate dynamics in the shortwave infrared that could potentially confound the seasonality of the broadband red, NIR, NDVI, and EVI2 measured by PAR and shortwave radiation sensors. However, bandwidth errors exhibited weak to non-existent relationships with solar position for broadband radiation derived indices across Imnaviat and the Fluxnet sites (Figures 5 and 1S; Table 1S). On the other hand, measurement bias sensitivity to solar zenith angle was an order of magnitude larger than that observed for broadband biases across both Imnaviat and Fluxnet sites (Figures 5; Figure 1S; Table 2S). The improved ability of radiation derived vegetation indices to replicate MODIS narrowband reflectance and VIs once solar position correction was applied provides strong evidence to attribute radiation derived biases to solar position, rather than bandwidth errors (Figures 7,8, 1S).

Here we used a simple machine learning empirically based model based on actual half hourly data to correct the seasonal biases in visible and NIR albedo. Our empirical model had high predictive power, explaining 85-95% of solar position biases, followed an expected BRDF response (i.e. a non-linear positive response with solar zenith angle), and included additional factors that may be difficult to parameterize in a BRDF model (Figure 6). For example, radiation sensors may have internal measurement biases due to solar position, known as a sensors cosine response (Blonquist et al. 2009; Ross and Sulev 2000). A sensor's cosine response describes how solar radiation is integrated across all solar zenith and azimuthal positions on a Lambertian receiver. This response differs among sensors and would be subject to measurement drift issues that would be difficult to quantify without additional information. Differences in a sensor's cosine response also may explain the differences in the sensitivity of radiation derived measurements to solar zenith angle among sites (Figures 4,8).

Quantifying and understanding measurement errors and limitations remains an important process in the scientific community (Kratzenberg et al. 2006; Richardson et al. 2008; Ross and Sulev

2000). This is especially true in ecosystem ecology as new, interdisciplinary, and automated remote- and near-sensing measurement techniques are being more commonly used. Understanding error sources and applying the proper corrections will result in improved understanding or quantification of ecosystem function. For example, the strong relationship between solar position corrected radiation derived vegetation indices and canopy photosynthesis demonstrate promise in using these data to fill long gaps in eddy covariance flux data. Moreover, the high correspondence between solar position corrected radiation- and satellite-derived vegetation indices indicates that these data can be valuable in gap filling MODIS data during cloudy periods (Figure 7). However, we caution future users of such data to also consider other potential important sources of measurement error, such as sensor drift and sensor spectral sensitivity, that may significantly alter the continuity of high quality radiation based vegetation indices (Kratzenberg et al. 2006; Ross and Sulev 2000). We encourage future work to implement, or improve upon, our methodology to gain further understanding the temporal dynamics of ecosystem C cycling and phenology with vegetation indices derived from solar and photosynthetically active radiation fluxes.

Acknowledgements

This work was supported by the National Science Foundation (NSF) grants #1065587 and #1026843 to the Marine Biological Laboratory, and NSF grants #1556772 to the University of Notre Dame. This work also was funded by the NSF division of Polar Programs Arctic Observatory Network grant numbers #856864, #1304271, #0632264, and #1107892. Any use of trade, product, or firm names is for descriptive purposes only and does not imply endorsement by the US Government.

Site Name	Latitude	Years	PFT	PAR Sensor	Pyranometer Sensor
Bondville[1]	40	2004-2007	Crop	Apogee	LI200
ARM SGP[1]	36.5	2004-2009	Crop	LI190	CM3
Sioux Falls[2]	43.2	2007-2009	Crop	NA	NA
UCI 1989[3]	55.9	2002-2005	Deciduous	LI190	CM3
UCI 1998[3]	56.5	2002-2005	Deciduous	LI190	CM3
Black Hills[4]	44.2	2004-2008	Evergreen	LI190	CM3
Flagstaff Managed[5]	35.1	2006-2009	Evergreen	BF3/LI190	CM3
UCI 1850[3]	55.9	2002-2005	Evergreen	LI190	CM3
UCI 1930[3]	55.9	2002-2005	Evergreen	LI190	CM3
UCI 1964[3]	55.9	2002-2005	Evergreen	LI190	CM3
UCI 1981[3]	55.9	2002-2005	Evergreen	LI190	CM3
Brookings[4]	44.3	2004-2010	Grassland	NA	NA
Canaan Valley[4]	39.1	2004-2010	Grassland	Apogee	CM3
Cottonwood[4]	43.9	2006-2009	Grassland	NA	NA
Flagstaff Wildfire[5]	35.4	2005-2009	Grassland	BF3/LI190	CM3
Fort Peck[4]	48.3	2002-2008	Grassland	LI190	Apogee
Goodwin Creek[4]	34.3	2002-2006	Grassland	Apogee	CM3
Kendall[6]	31.7	2004-2009	Grassland	NA	NA
Audubon[4]	31.8	2004-2009	Grassland	LI190	CM3
Ivotuk[7]	68.5	2004-2006	Tundra	LI190	CM3
Imnaviat[8]	68.6	2009-2011	Tundra	LI190	CM3
Unburned[9]	68.9	2008-2011	Tundra	LI190	CM3
Severe[9]	68.9	2008-2011	Tundra	LI190	CM3
Moderate[9]	68.9	2008-2011	Tundra	LI190	CM3
Santa Rita Mesquite[10]	31.8	2004-2007	Grassland/ Shrub	NA	NA

Table 1. Site names, location, years, Plant Functional Type (PFT) and sensors used at each of the sites used in this study. [1]Hollinger et al. (1994); [2]Verma et al. (2005); [3]Goulden et al. (2011); [4]Wilson and Myers (2007); [5]Dore et al. (2016); [6]Scott et al. (2010); [7]McEwing et al. (2015); [8]This study; [9]Rocha and Shaver (2011); [10]Scott et al. (2009)

	Spectroradiometer v. MODIS *R^2 [MAE]*	**Spectroradiometer v. Radiation** *R^2 [MAE]*	**MODIS v. Radiation** *R^2 [MAE]*
Red	0.22 [0.01]	0.21 [0.01]	0.19 [0.01]
NIR	0.17 [0.03]	0.20 [0.03]	0.22 [0.03]
EVI2	0.67 [0.03]	0.42 [0.09]	0.42 [0.05]
NDVI	0.55 [0.05]	0.34 [0.11]	0.34 [0.05]

Table 2. R-squared and Mean Absolute Error (MAE) of relationships among spectroradiometer-, MODIS-, uncorrected radiation- derived reflectance and vegetation indices.

	MODIS v. U-Radiation *R^2 [MAE]*	**MODIS v. C-Radiation** *R^2 [MAE]*
Red	0.19 [0.01]	0.19 [0.01]
NIR	0.22 [0.03]	0.47 [0.02]
EVI2	0.42 [0.05]	0.56 [0.03]
NDVI	0.34 [0.05]	0.56 [0.03]

Table 3. R-squared and Mean Absolute Error (MAE) of relationships among MODIS- , uncorrected (U) radiation-, and corrected (C) radiation- derived reflectance and vegetation indices.

Figure 1: Mean Absolute Error (MAE {unitless VI ratios}: blue circles left y-axis) and r-squared (R^2{unitless}: red triangles right y-axis) of the relationship between spectroradiometer- and MODIS- derived NDVI (top) and EVI2 (bottom) at different MODIS spatial integration scales at Imnaviat.

Figure 2: Seasonal cycle of spectroradiometer- (black diamonds), radiation- (blue dots), and MODIS-derived (red dots) red (A) and near-infrared (B) reflectances, and NDVI (C) and EVI2 (D) from quality controlled 2008-2018 Imnaviat data.

Figure 3: Dependence of MODIS- and radiation- derived differences on solar zenith angle for red reflectance (A), near infrared reflectance (B), NDVI (C), and EVI2 (D) at Imnaviat. Regression lines indicate significant relationships at the 95% confidence level.

Figure 4: Dependence of MODIS- and radiation- derived differences on solar zenith angle for red reflectance (A), near infrared reflectance (B), NDVI (C), and EVI2 (D) from Fluxnet sites across biome types. Lines in panels C and D are only for statistically significant relationships at the 95% confidence level.

Figure 5: Dependence of ground based spectroradiometer broad- and narrow-band derived differences (i.e. broadband-narrowband) on solar zenith angle for red reflectance (A), near infrared reflectance (B), NDVI (C), and EVI2 (D) at Imnaviat. Regression lines indicate significant relationships at the 95% confidence level.

Figure 6: The correction factor dependence on solar zenith angle for visible (solid dots) and near infrared (open dots) albedo. The inset plot shows seasonal changes in daily averaged solar zenith angle (solid line) and daily averaged azimuth angle (dotted line). The grey highlighted area denotes the growing season period at Imnaviat.

Figure 7: Correspondence between radiation- and MODIS- derived red (A) and near infrared (B) reflectances, and NDVI (C) and EVI2 (D) at Imnaviat. Grey dots are MODIS and uncorrected radiation derived reflectance and indices, whereas triangles are MODIS and radiation derived reflectance and indices that were corrected for solar position biases.

Figure 8: Average percent change in the Mean Absolute Error (MAE) between MODIS satellite- and radiation-derived NDVI (black bars) and EVI2 (grey bars) relative to the uncorrected values at the Fluxnet sites. Fluxnet sites were grouped by ecosystem type, and error bars represent standard errors.

Figure 9: Relationship between Imnaviat Gross Ecosystem Exchange (GEE) and solar position corrected (open triangles) and uncorrected (grey circles) radiation derived vegetation indices. NDVI-GEE relationships are in left panel (A), whereas EVI2-GEE are in right panel (B). The solid line represents the correlation between the solar position corrected vegetation index and GEE, whereas the dotted line represents the correlation between uncorrected vegetation indices and GEE. Hatched arrows in left panel represent the hysteresis in the relationship between uncorrected NDVI and GEE, while numbers represent the day of year of each observation.

Figure 10: Mean Absolute Error (MAE) of the start-(SOS), length-(LOS), and end-(EOS) of the growing season derived from MODIS- (black bar), uncorrected radiation- (grey), and solar position corrected radiation- (dark grey) derived NDVI (A) and EVI2 (B) at Imnaviat.

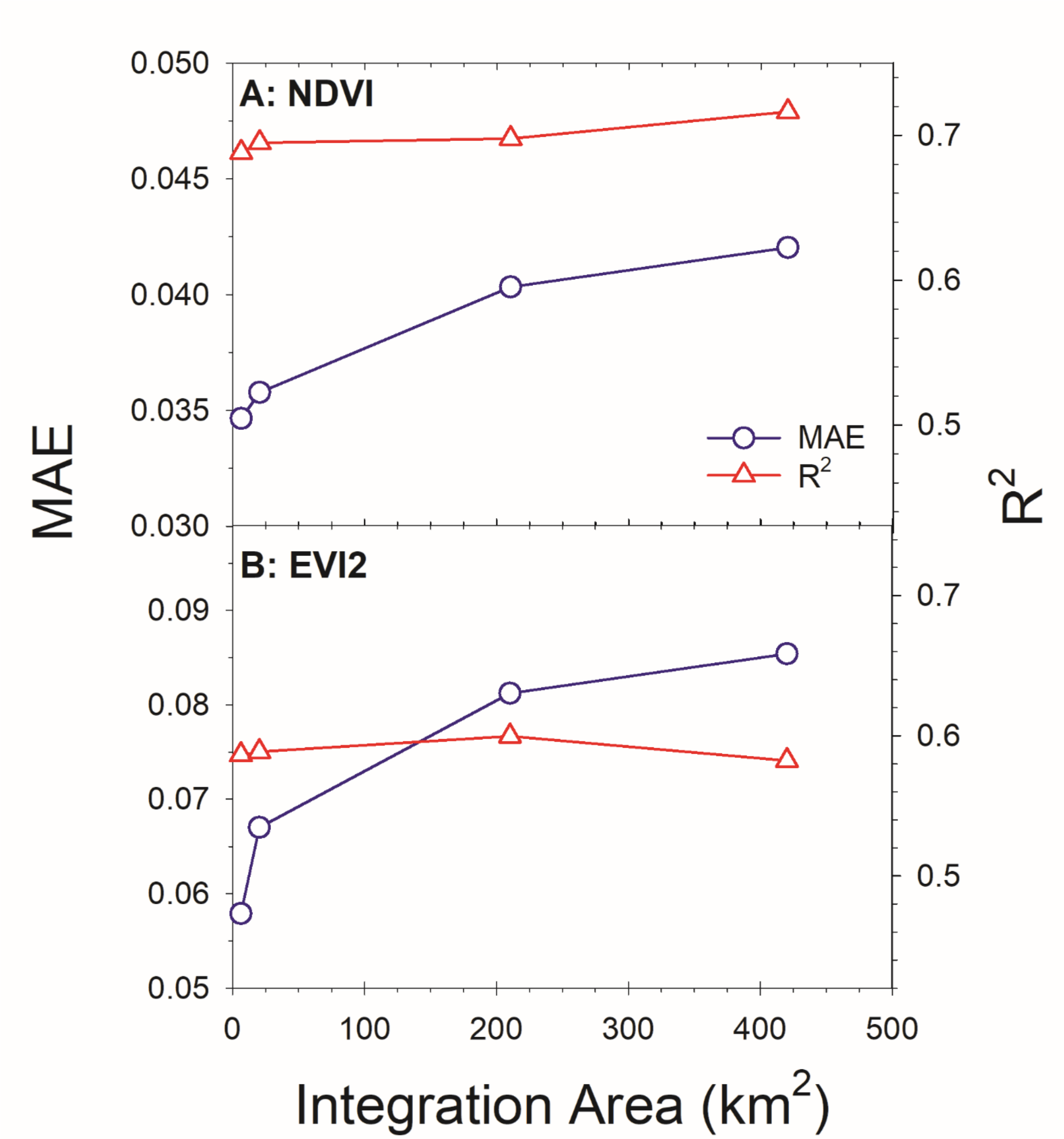
A: NDVI
B: EVI2
MAE
R^2
0.050
0.045
0.040
0.035
0.030
0.09
0.08
0.07
0.06
0.05
0.7
0.6
0.5
0
100
200
300
400
500
Integration Area (km^2)

Figure 1.

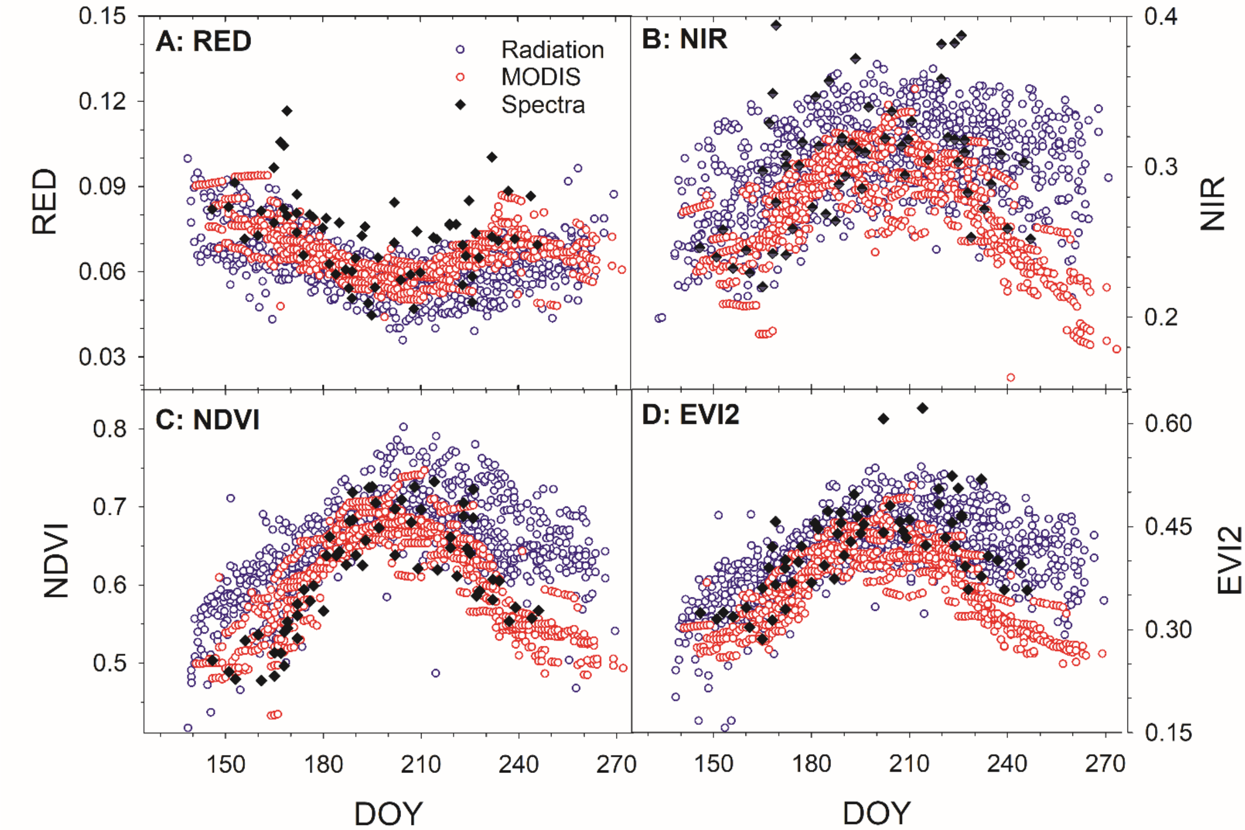
A: RED
B: NIR
C: NDVI
D: EVI2
Radiation
MODIS
Spectra
RED
NIR
NDVI
EVI2
0.15
0.12
0.09
0.06
0.03
0.4
0.3
0.2
0.8
0.7
0.6
0.5
0.60
0.45
0.30
0.15
150
180
210
240
270
DOY

Figure 2.

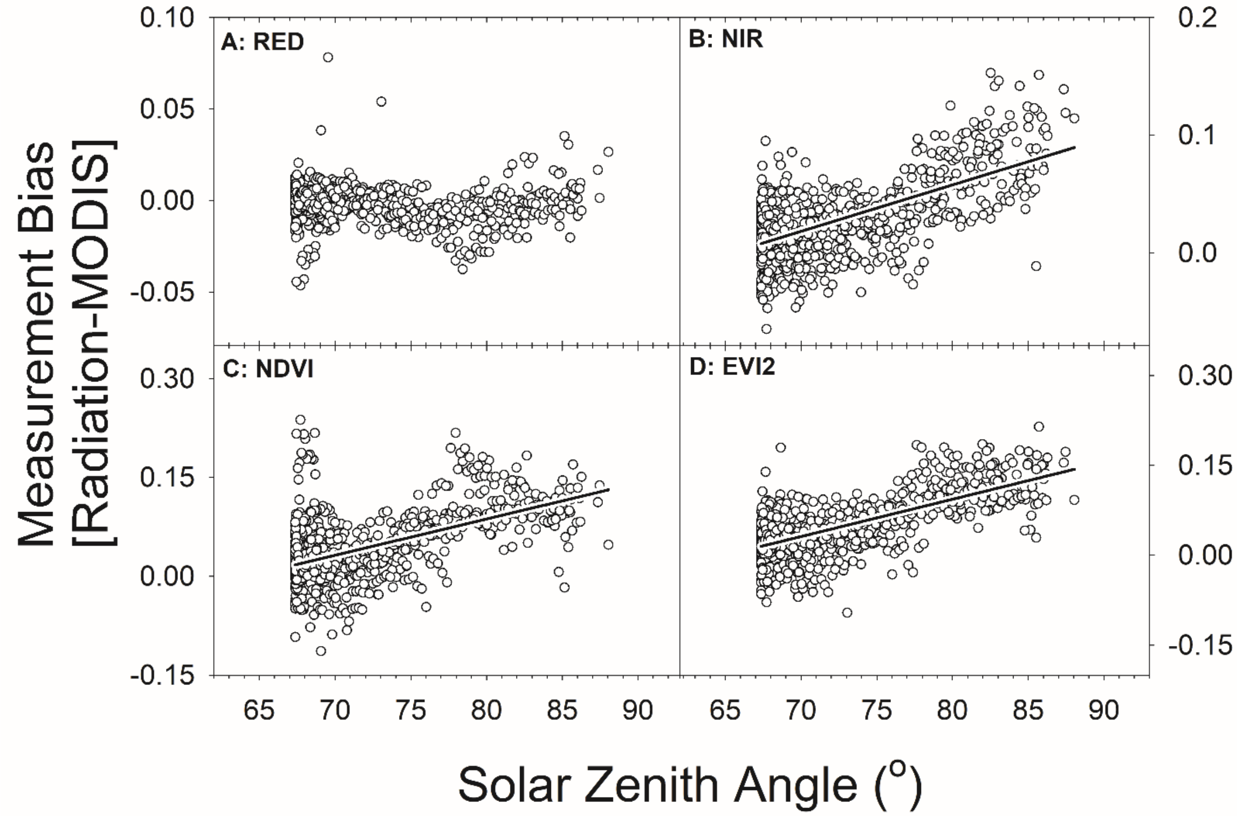
A: RED
B: NIR
C: NDVI
D: EVI2
Measurement Bias [Radiation-MODIS]
Solar Zenith Angle (°)
0.10
0.05
0.00
-0.05
0.2
0.1
0.0
0.30
0.15
0.00
-0.15
65
70
75
80
85
90

Figure 3.

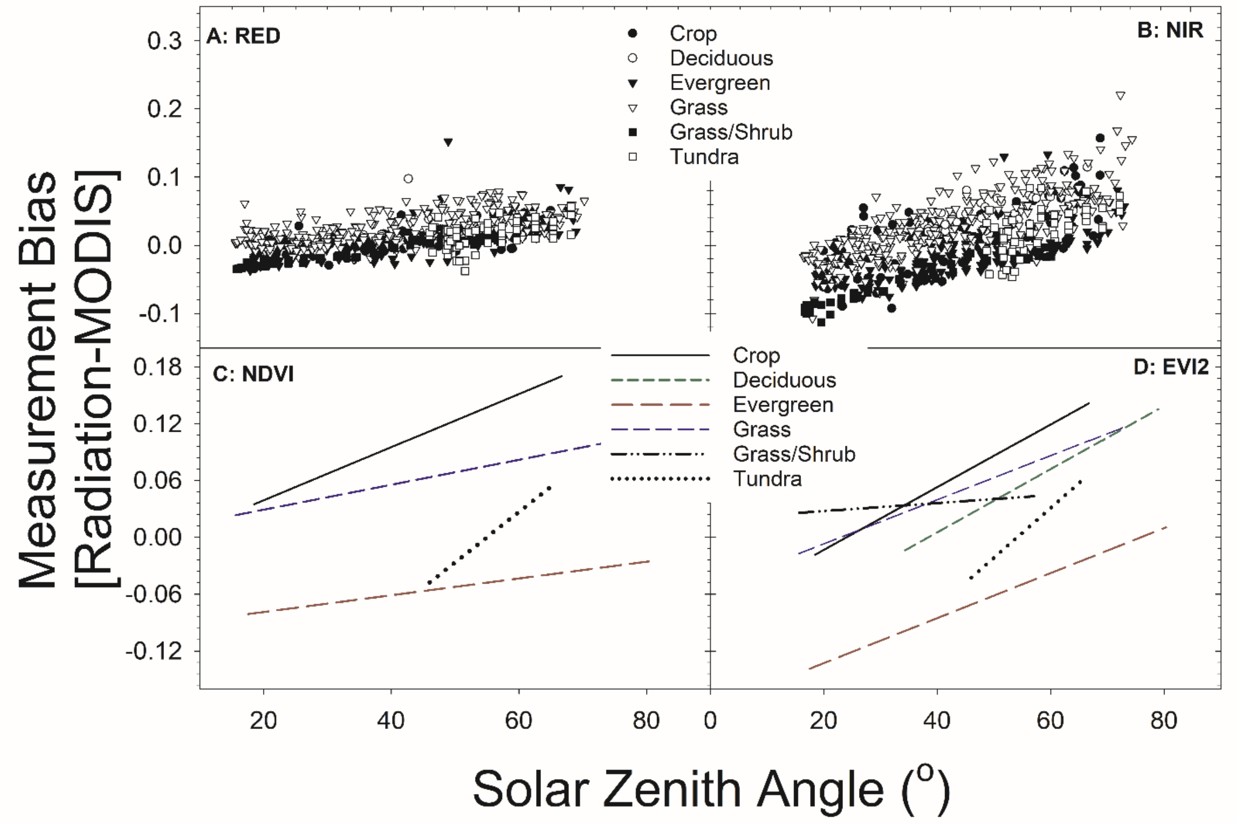
A: RED
B: NIR
C: NDVI
D: EVI2
Crop
Deciduous
Evergreen
Grass
Grass/Shrub
Tundra
Measurement Bias [Radiation-MODIS]
0.3
0.2
0.1
0.0
-0.1
0.18
0.12
0.06
0.00
-0.06
-0.12
20
40
60
80
0
Solar Zenith Angle (o)

Figure 4.

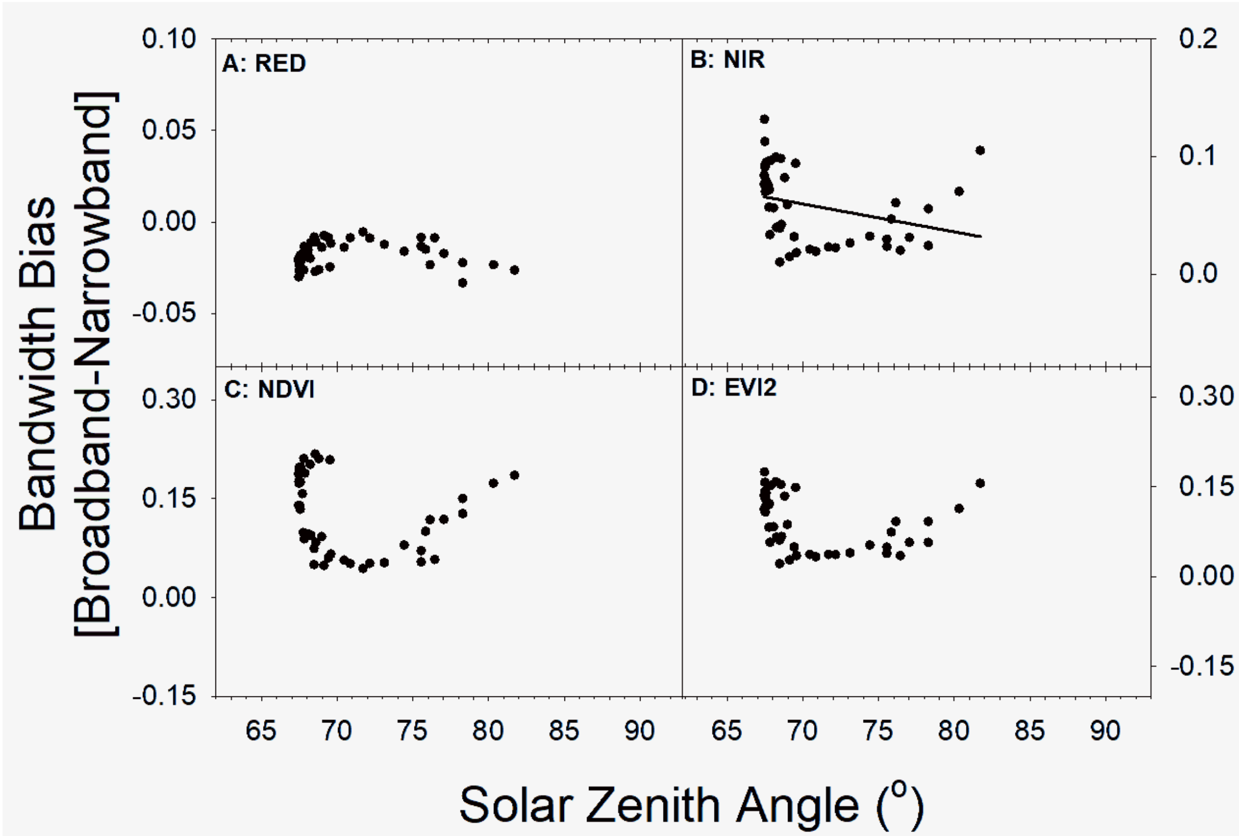
A: RED
B: NIR
C: NDVI
D: EVI2
Bandwidth Bias
[Broadband-Narrowband]
Solar Zenith Angle (°)
0.10
0.05
0.00
-0.05
0.30
0.15
0.00
-0.15
0.2
0.1
0.0
0.30
0.15
0.00
-0.15
65
70
75
80
85
90
65
70
75
80
85
90

Figure 5.

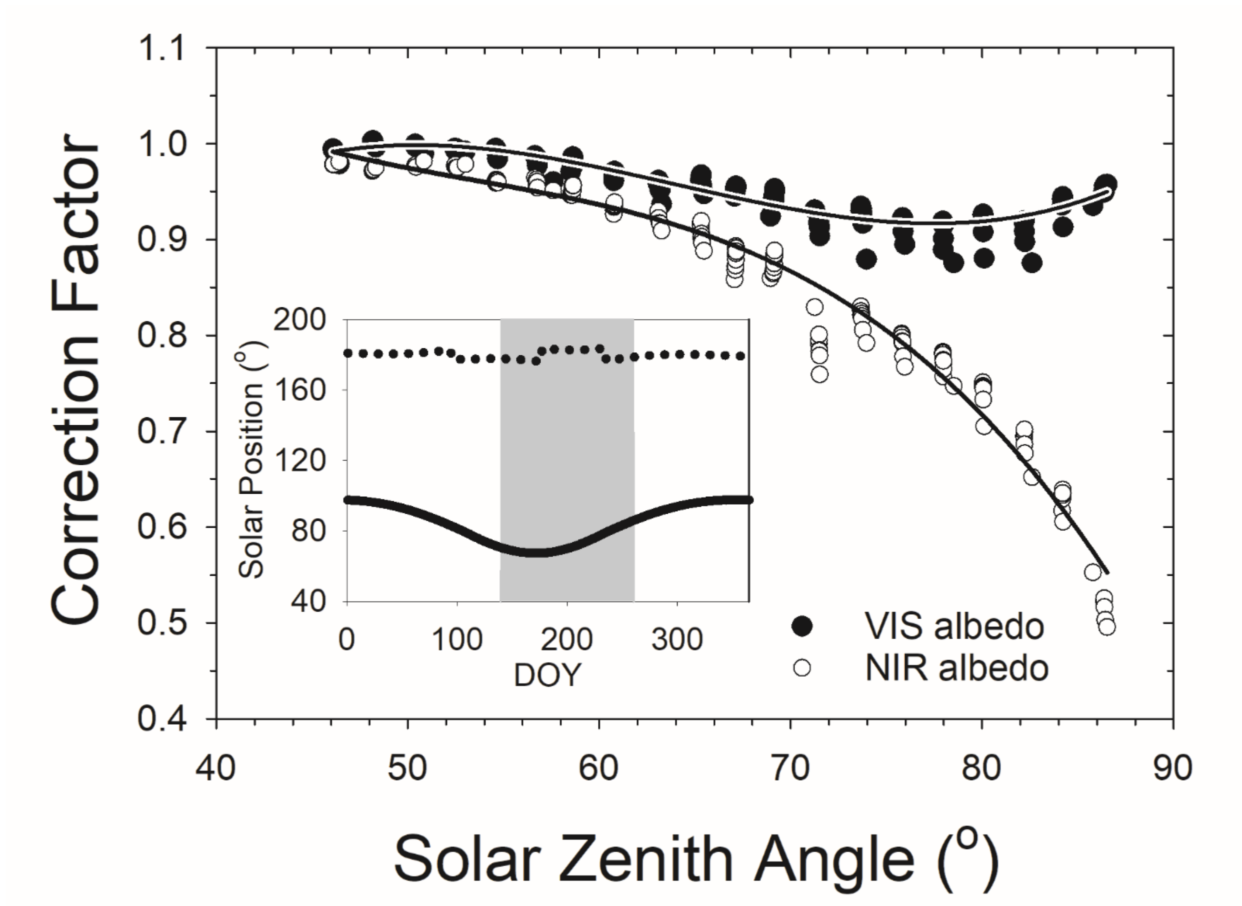
Correction Factor
1.1
1.0
0.9
0.8
0.7
0.6
0.5
0.4
40
50
60
70
80
90
Solar Zenith Angle (o)
Solar Position (o)
200
160
120
80
40
0
100
200
300
DOY
VIS albedo
NIR albedo

Figure 6.

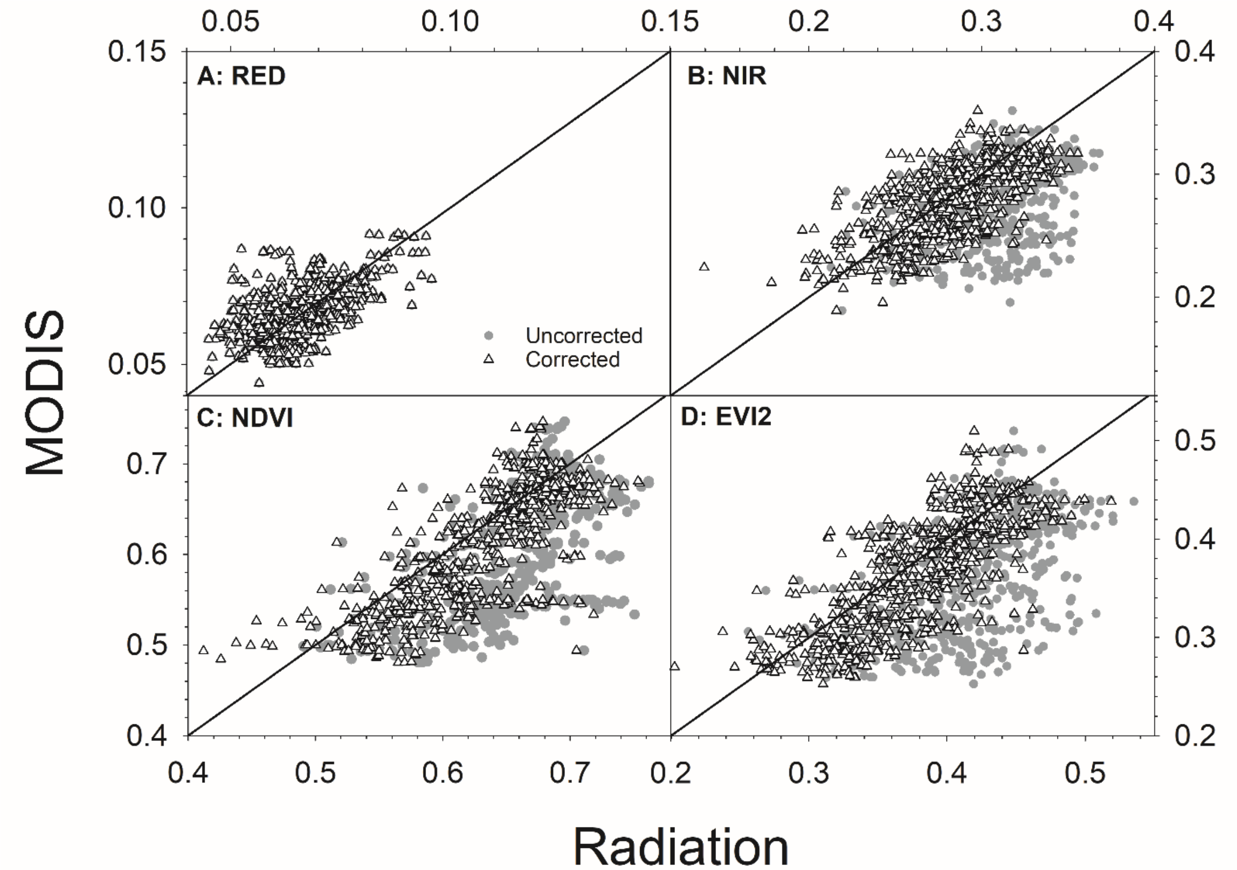
A: RED
B: NIR
C: NDVI
D: EVI2
Uncorrected
Corrected
MODIS
Radiation
0.05
0.10
0.15
0.2
0.3
0.4
0.5
0.6
0.7

Figure 7.

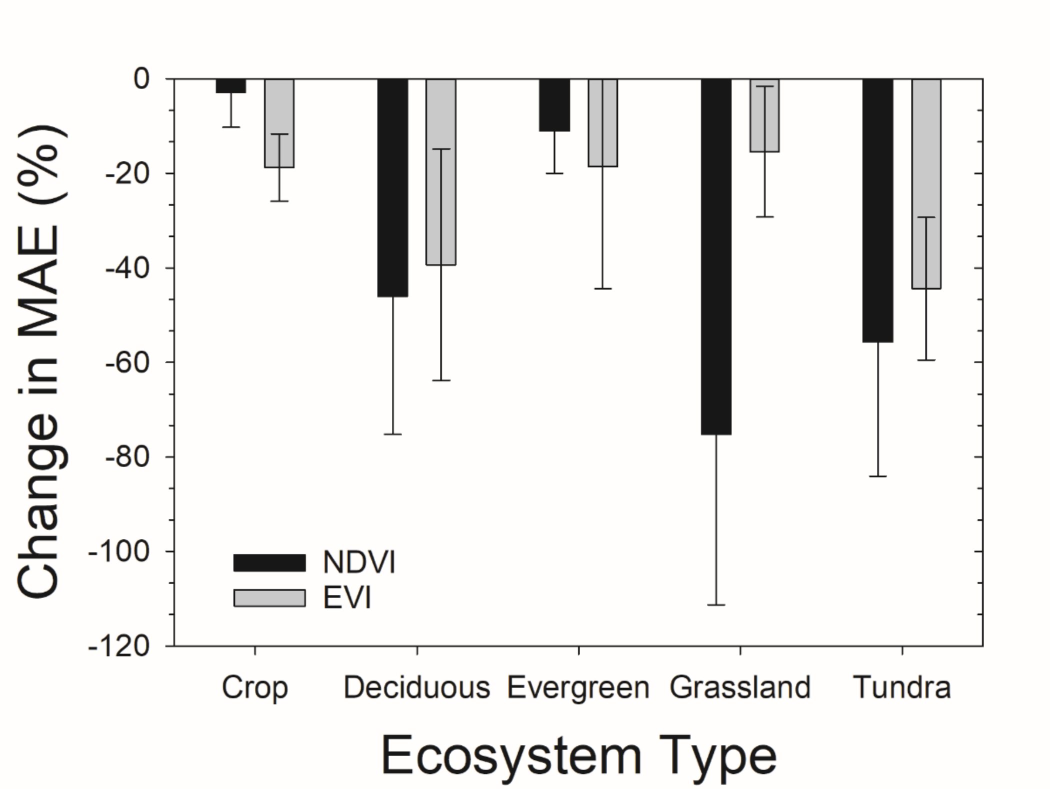

0
-20
-40
-60
-80
-100
-120
Change in MAE (%)
NDVI
EVI
Crop
Deciduous
Evergreen
Grassland
Tundra
Ecosystem Type

Figure 8.

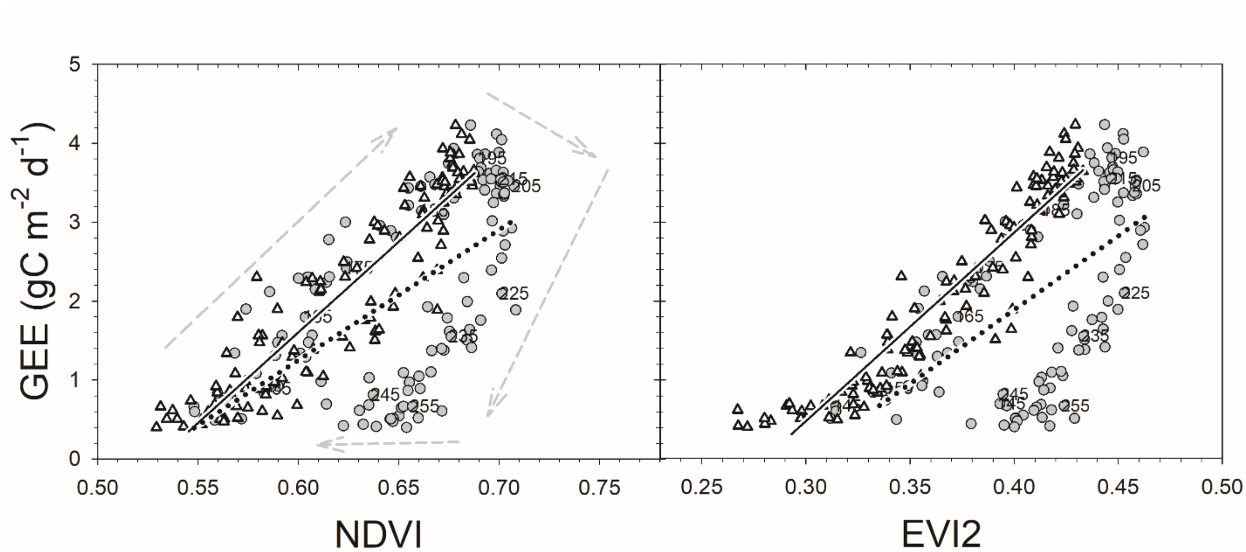
GEE (gC m-2 d-1)
NDVI
EVI2
0.50
0.55
0.60
0.65
0.70
0.75
0.25
0.30
0.35
0.40
0.45
0.50
0
1
2
3
4
5
195
205
215
225
255
245
165

Figure 9.

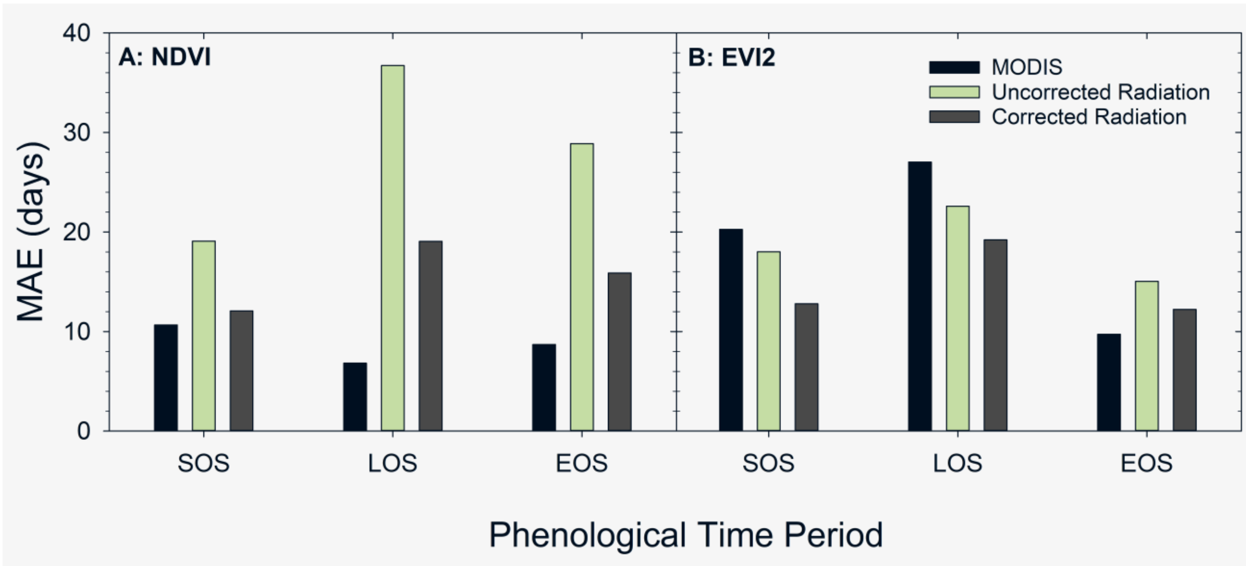

A: NDVI
B: EVI2
MODIS
Uncorrected Radiation
Corrected Radiation
MAE (days)
0
10
20
30
40
SOS
LOS
EOS
SOS
LOS
EOS
Phenological Time Period

Figure 10.

Supplement:

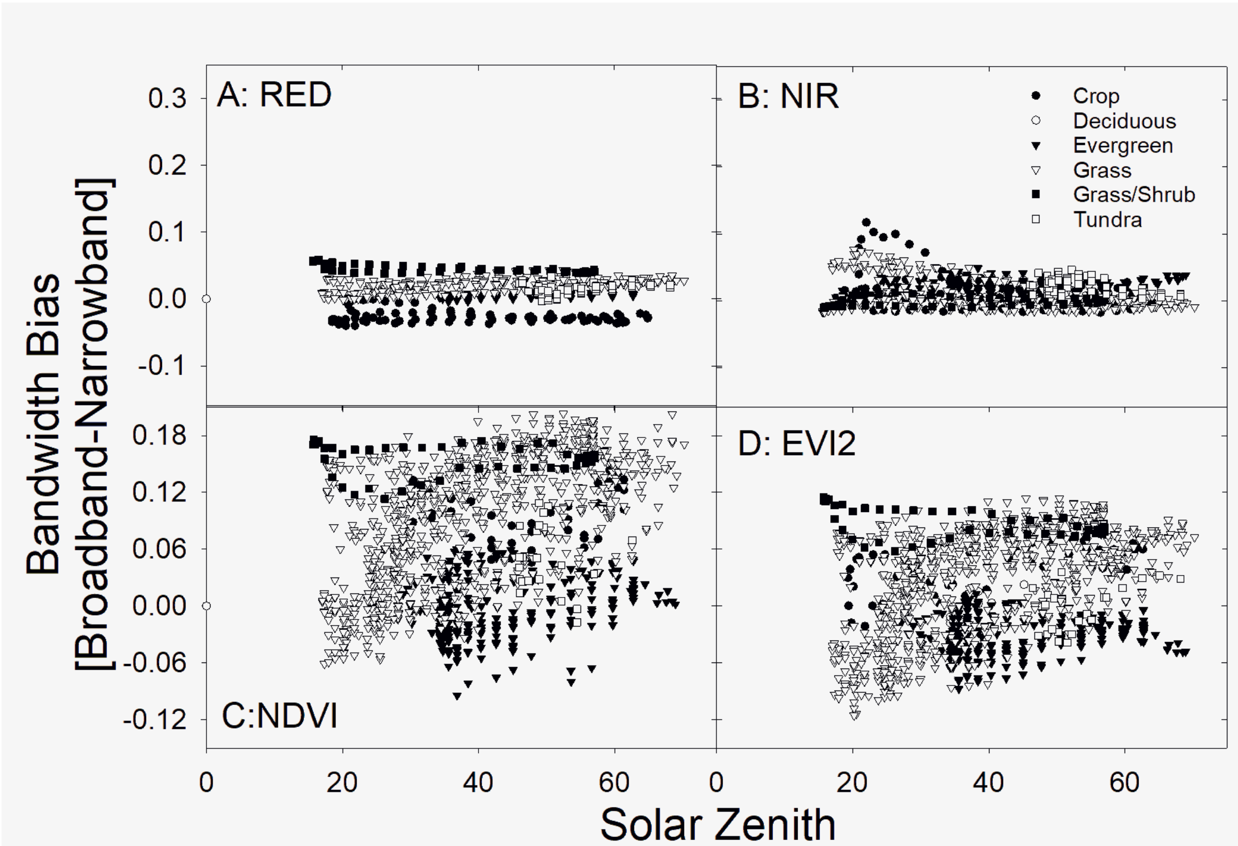

Figure 1S: Dependence of bandwidth biases (broadband-narrowband) derived differences on solar zenith angle for red reflectance (A), near infrared reflectance (B), NDVI (C), and EVI2 (D) from Fluxnet sites across biome types. Note that the y-axes are scaled to be the same as those observed in Figure 4.

Table 1S: Summary statistics for bandwidth bias correlation with solar zenith angle in Figure 1S. The number represents the R^2 of the relationship, while the number in [brackets] represents the sensitivity to solar zenith angle measured as the slope of the line.

PFT	Red (R^2 [Slope])	NIR (R^2 [Slope])	NDVI (R^2 [Slope])	EVI2 (R^2 [Slope])
Crop	**0.06 [-0.0001]**	**0.09 [-0.0005]**	0.01 [0.0002]	**0.37 [-0.0007]**
Deciduous	**0.46 [-0.0003]**	**0.14 [-0.0006]**	0.03 [0.0003]	**0.52 [-0.0046]**
Evergreen	**0.06 [0.0001]**	**0.12 [0.0003]**	**0.06 [0.00093]**	0.02 [0.0003]
Grass	**0.62 [0.0002]**	**0.11 [-0.0006]**	**0.06 [0.0009]**	**0.29 [0.002]**
Grass/Shrub	**0.10 [0.0001]**	**0.08 [-0.0005]**	0.01 [0.00003]	**0.22 [-0.0005]**
Tundra	**0.16 [0.0005]**	**0.22 [-0.0008]**	0.01 [-0.0001]	**0.29 [0.002]**

*Numbers in bold represent statistically significant relationships at the 95% Confidence level.

References:

Baldocchi, D.D. (2003). Assessing the eddy covariance technique for evaluating carbon dioxide exchange rates of ecosystems: past, present and future. *Global Change Biology, 9*, 479-492

Balzarolo, M., Anderson, K., Nichol, C., Rossini, M., Vescovo, L., Arriga, N., Wohlfahrt, G., Calvet, J.-C., Carrara, A., Cerasoli, S., Cogliati, S., Daumard, F., Eklundh, L., Elbers, J.A., Evrendilek, F., Handcock, R.N., Kaduk, J., Klumpp, K., Longdoz, B., Matteucci, G., Meroni, M., Montagnani, L., Ourcival, J.-M., Sánchez-Cañete, E.P., Pontailler, J.-Y., Juszczak, R., Scholes, B., & Martín, M.P. (2011). Ground-based optical measurements at European flux sites: a review of methods, instruments and current controversies. *Sensors (Basel, Switzerland), 11*, 7954-7981

Beck, P.S.A., Atzberger, C., Høgda, K.A., Johansen, B., & Skidmore, A.K. (2006). Improved monitoring of vegetation dynamics at very high latitudes: A new method using MODIS NDVI. *Remote Sensing of Environment, 100*, 321-334

Bhandari, S., Phinn, S., & Gill, T. (2011). Assessing viewing and illumination geometry effects on the MODIS vegetation index (MOD13Q1) time series: implications for monitoring phenology and disturbances in forest communities in Queensland, Australia. *International Journal of Remote Sensing, 32*, 7513-7538

Blonquist, J.M., Tanner, B.D., & Bugbee, B. (2009). Evaluation of measurement accuracy and comparison of two new and three traditional net radiometers. *Agricultural and Forest Meteorology, 149*, 1709-1721

Carroll, J.J., & Fitch, B.W. (1981). Effects of solar elevation and cloudiness on snow albedo at the South Pole. *Journal of Geophysical Research: Oceans, 86*, 5271-5276

Dore, S., Montes-Helu, M., Hart, S.C., Hungate, B.A., Koch, G.W., Moon, J.B., Finkral, A.J., & Kolb, T.E. (2012). Recovery of ponderosa pine ecosystem carbon and water fluxes from thinning and stand-replacing fire. *Global Change Biology, 18*, 3171-3185

Disney, M., Lewis, P., Thackrah, G., Quaife, T., & Barnsley, M. (2004). Comparison of MODIS broadband albedo over an agricultural site with ground measurements and values derived from Earth observation data at a range of spatial scales. *International Journal of Remote Sensing, 25*, 5297-5317

Euskirchen, E.S., Bret-Harte, M.S., Scott, G.J., Edgar, C., & Shaver, G.R. (2012). Seasonal patterns of carbon dioxide and water fluxes in three representative tundra ecosystems in northern Alaska. *Ecosphere, 3*, art4

Euskirchen, E.S., Bret-Harte, M.S., Shaver, G.R., Edgar, C.W., & Romanovsky, V.E. (2017). Long-Term Release of Carbon Dioxide from Arctic Tundra Ecosystems in Alaska. *Ecosystems, 20*, 960-974

Fisher, J.I., Mustard, J.F., & Vadeboncoeur, M.A. (2006). Green leaf phenology at Landsat resolution: Scaling from the field to the satellite. *Remote Sensing of Environment, 100*, 265-279

Fisher, J.I., Richardson, A.D., & Mustard, J.F. (2007). Phenology model from surface meteorology does not capture satellite-based greenup estimations. *Global Change Biology, 13*, 707-721

Gamon, J.A., Coburn, C., Flanagan, L.B., Huemmrich, K.F., Kiddle, C., Sanchez-Azofeifa, G.A., Thayer, D.R., Vescovo, L., Gianelle, D., Sims, D.A., Rahman, A.F., & Pastorello, G.Z. (2010). SpecNet revisited: bridging flux and remote sensing communities. *Canadian Journal of Remote Sensing, 36*, S376-S390

Gamon, J.A., Rahman, A.F., Dungan, J.L., Schildhauer, M., & Huemmrich, K.F. (2006). Spectral Network (SpecNet)—What is it and why do we need it? *Remote Sensing of Environment, 103*, 227-235

Huemmrich, K.F., T.A. Black, P.G. Jarvis, J.H. McCaughey, F.G. Hall (1999). High temporal resolution NDVI phenology from micrometeorological radiation sensors. *Journal of Geophysical Research: Atmospheres, 104*, 27935-27944

Goulden, M.L., Winston, G.C., McMillan, A.M.S., Litvak, M.E., Read, E.L., Rocha, A.V., & Rob Elliot, J. (2006). An eddy covariance mesonet to measure the effect of forest age on land–atmosphere exchange. *Global Change Biology, 12*, 2146-2162

Hollinger, S.E., Beth, C., Reinke, and R.A. Peppler (1994). Illinois Climate Network: Site Descriptions, Instrumentation, and Data Management In C. Illinois State Water Survey, IL (Ed.) (p. 62)

Huete, A.R. (1987). Soil and Sun angle interactions on partial canopy spectra. *International Journal of Remote Sensing, 8*, 1307-1317

Jenkins, J.P., Richardson, A., Braswell, B., Ollinger, S.V., Hollinger, D., & Smith, M.-L. (2007). Refining Light-Use Efficiency Calculations for a Deciduous Forest Canopy Using Simultaneous Tower-Based Carbon Flux and Radiometric Measurements. *Agricultural and Forest Meteorology, 143*, 64-79

Jiang, Z., Huete, A., Didan, K., & Miura, T. (2008). *Development of a two-band enhanced vegetation index without a blue band*.

Kratzenberg, M.G., Beyer, H.G., Colle, S., & Albertazzi, A. (2006). Uncertainty Calculations in Pyranometer Measurements and Application, 689-698

Kriebel, K.T. (1979). Albedo of vegetated surfaces: its variability with differing irradiances. *Remote Sensing of Environment, 8*, 283-290

Liang, S. (2000). Narrowband to broadband conversions of land surface albedo I Algorithms. *Remote Sensing of Environment*, 76, 213-238.

Ma, X., Huete, A., & Tran, N.N. (2019). Interaction of Seasonal Sun-Angle and Savanna Phenology Observed and Modelled using MODIS. *Remote Sensing, 11*

McEwing, K.R., Fisher, J.P., & Zona, D. (2015). Environmental and vegetation controls on the spatial variability of CH4 emission from wet-sedge and tussock tundra ecosystems in the Arctic. *Plant and Soil, 388*, 37-52

Middleton, E.M. (1992). Quantifying reflectance anisotropy of photosynthetically active radiation in grasslands. *Journal of Geophysical Research: Atmospheres, 97*, 18935-18946

Myers, D.R. (2017). *Solar radiation: Practical modeling for renewable energy applications*. Boca Raton: CRC Press, https://doi.org/10.1201/b13898

Rahman, H., Verstraete, M.M., & Pinty, B. (1993). Coupled surface-atmosphere reflectance (CSAR) model: 1. Model description and inversion on synthetic data. *Journal of Geophysical Research: Atmospheres, 98*, 20779-20789

Ramsey, F.L.S., D.W. (2013). The statistical sleuth: A course in methods of data analysis. *Boston: Brooks/Cole, Cengage*

Richardson, A.D., Mahecha, M.D., Falge, E., Kattge, J., Moffat, A.M., Papale, D., Reichstein, M., Stauch, V.J., Braswell, B.H., Churkina, G., Kruijt, B., & Hollinger, D.Y. (2008). Statistical properties of random CO2 flux measurement uncertainty inferred from model residuals. *Agricultural and Forest Meteorology, 148*, 38-50

Rocha, A.V., & Shaver, G.R. (2009). Advantages of a two band EVI calculated from solar and photosynthetically active radiation fluxes. *Agricultural and Forest Meteorology, 149*, 1560-1563

Rocha, A.V., & Shaver, G.R. (2011). Burn severity influences postfire CO_2 exchange in arctic tundra. *Ecological Applications, 21*, 477-489

Ross, J., & Sulev, M. (2000). Sources of errors in measurements of PAR. *Agricultural and Forest Meteorology, 100*, 103-125

Rouse, J.W., Jr., R.H. Haas, D.W. Deering, J.A. Schell, and J.C. Haran (1974). Monitoring the vernal advancement and retrogradation (Green Wave Effect) of Natural Vegetation [Great Plains Cooridor]. *Earth Resources and Remote Sensing*

Schaaf, C.B., Gao, F., Strahler, A.H., Lucht, W., Li, X., Tsang, T., Strugnell, N.C., Zhang, X., Jin, Y., Muller, J.-P., Lewis, P., Barnsley, M., Hobson, P., Disney, M., Roberts, G., Dunderdale, M., Doll, C., d'Entremont, R.P., Hu, B., Liang, S., Privette, J.L., & Roy, D. (2002). First operational BRDF, albedo nadir reflectance products from MODIS. *Remote Sensing of Environment, 83*, 135-148

Schaepman-Strub, G., Schaepman, M.E., Painter, T.H., Dangel, S., & Martonchik, J.V. (2006). Reflectance quantities in optical remote sensing—definitions and case studies. *Remote Sensing of Environment, 103*, 27-42

Schmid, H.P. (1997). Experimental design for flux measurements: matching scales of observations and fluxes. *Agricultural and Forest Meteorology, 87*, 179-200

Scott, R.L., Hamerlynck, E.P., Jenerette, G.D., Moran, M.S., & Barron-Gafford, G.A. (2010). Carbon dioxide exchange in a semidesert grassland through drought-induced vegetation change. *Journal of Geophysical Research: Biogeosciences, 115*

Shuai, Y., Schaaf, C., Zhang, X., Strahler, A., Roy, D., Morisette, J., Wang, Z., Nightingale, J., Nickeson, J., Richardson, A.D., Xie, D., Wang, J., Li, X., Strabala, K., & Davies, J.E. (2013). Daily MODIS 500 m reflectance anisotropy direct broadcast (DB) products for monitoring vegetation phenology dynamics. *International Journal of Remote Sensing, 34*, 5997-6016

Sims, D.A., Rahman, A.F., Cordova, V.D., El-Masri, B.Z., Baldocchi, D.D., Flanagan, L.B., Goldstein, A.H., Hollinger, D.Y., Misson, L., Monson, R.K., Oechel, W.C., Schmid, H.P., Wofsy, S.C., & Xu, L. (2006). On the use of MODIS EVI to assess gross primary productivity of North American ecosystems. *Journal of Geophysical Research: Biogeosciences, 111*

Sims, D.A., Rahman, A.F., Vermote, E.F., & Jiang, Z. (2011). Seasonal and inter-annual variation in view angle effects on MODIS vegetation indices at three forest sites. *Remote Sensing of Environment, 115*, 3112-3120

Stoy, P.a.D., MC and Richardson, AD and Vargas, R and Barr, AG and Anderson, RS and Arain, MA and Baker, IT and Black, TA and Chen, JM and Cook, RB and Gough, CM and Grant, RF and Hollinger, DY and Izaurralde, RC and Kucharik, CJ and Lafleur, P and Law, BE and Liu, S and Lokupitiya, E and Luo, Y and Munger, JW and Peng, C and Poulter, B and Price, DT and Ricciuto, DM and Riley, WJ and Sahoo, AK and Schaefer, K and Schwalm, CR and Tian, H and Verbeeck, Hans and Weng, E (2013). Evaluating the agreement between measurements and models of net ecosystem exchange at different times and timescales using wavelet coherence: an example using data from the North American Carbon Program Site-Level Interim Synthesis. *Biogeosciences, 10*, 6893-6909

Tittebrand, A., U. Spank, C.H. Bernhofer (2009). Comparison of satellite- and ground-based NDVI above different land-use types. *Theoretical and Applied Climatology, 98*, 171-186

Ueyama, M., Iwata, H., Harazono, Y., Euskirchen, E.S., Oechel, W.C., & Zona, D. (2013). Growing season and spatial variations of carbon fluxes of Arctic and boreal ecosystems in Alaska (USA). *Ecological Applications, 23*, 1798-1816

Verma, S.B., Dobermann, A., Cassman, K.G., Walters, D.T., Knops, J.M., Arkebauer, T.J., Suyker, A.E., Burba, G.G., Amos, B., Yang, H., Ginting, D., Hubbard, K.G., Gitelson, A.A., &

Walter-Shea, E.A. (2005). Annual carbon dioxide exchange in irrigated and rainfed maize-based agroecosystems. *Agricultural and Forest Meteorology, 131*, 77-96

Wang, Q., Tenhunen, J., Dinh, N.Q., Reichstein, M., Vesala, T., & Keronen, P. (2004). Similarities in ground- and satellite-based NDVI time series and their relationship to physiological activity of a Scots pine forest in Finland. *Remote Sensing of Environment, 93*, 225-237

Wang, X., & Zender, C.S. (2010). Constraining MODIS snow albedo at large solar zenith angles: Implications for the surface energy budget in Greenland. *Journal of Geophysical Research: Earth Surface, 115*

Wang, Z., Barlage, M., Zeng, X., Dickinson, R.E., & Schaaf, C.B. (2005). The solar zenith angle dependence of desert albedo. *Geophysical Research Letters, 32*

Wang, Z., Schaaf, C.B., Chopping, M.J., Strahler, A.H., Wang, J., Román, M.O., Rocha, A.V., Woodcock, C.E., & Shuai, Y. (2012). Evaluation of Moderate-resolution Imaging Spectroradiometer (MODIS) snow albedo product (MCD43A) over tundra. *Remote Sensing of Environment, 117*, 264-280

Wilson, T.B., & Meyers, T.P. (2007). Determining vegetation indices from solar and photosynthetically active radiation fluxes. *Agricultural and Forest Meteorology, 144*, 160-179

Wittich, K.-P., & Kraft, M. (2008). The normalised difference vegetation index obtained from agrometeorological standard radiation sensors: a comparison with ground-based multiband spectroradiometer measurements during the phenological development of an oat canopy. *International Journal of Biometeorology, 52*, 167-177

Wohlfahrt, G., Pilloni, S., Hörtnagl, L., & Hammerle, A. (2010). Estimating carbon dioxide fluxes from temperate mountain grasslands using broad-band vegetation indices. *Biogeosciences (Online), 7*, 683-694

Wright, K.S., & Rocha, A.V. (2018). A test of functional convergence in carbon fluxes from coupled C and N cycles in Arctic tundra. *Ecological Modelling, 383*, 31-40

Xiao, X., Zhang, Q., Hollinger, D., Aber, J., & Moore Iii, B. (2005). Modeling gross primary production of an evergreen needleleaf forest using MODIS and climate data. *Ecological Applications, 15*, 954-969

Yang, F., Mitchell, K., Hou, Y.-T., Dai, Y., Zeng, X., Wang, Z., & Liang, X.-Z. (2008). Dependence of Land Surface Albedo on Solar Zenith Angle: Observations and Model Parameterization. *Journal of Applied Meteorology and Climatology, 47*, 2963-2982

Solar position confounds the relationship between ecosystem function and vegetation indices derived from solar and photosynthetically active radiation fluxes.

Adrian V. Rocha[1], Rose Appel[1], M. Syndonia Bret-Harte[2], Eugenie Euskirchen[2], Verity Salmon[3], Gaius Shaver[4]

[1]Department of Biological Sciences and the Environmental Change Initiative, Notre Dame, IN 46556, USA

[2]Institute of Arctic Biology, University of Alaska Fairbanks, Fairbanks, AK 99775, USA

[3]Environmental Sciences Division and Climate Change Science Institute, Oak Ridge National Laboratory, Oak Ridge, TN 37831, USA

[4]The Ecosystems Center, Marine Biological Laboratory, Woods Hole, MA 02543, USA

Submitted to: Agricultural and Forest Meteorology

Corresponding Author:
Adrian V. Rocha
University of Notre Dame
Department of Biological Sciences and the Environmental Change Initiative
100 Galvin Life Sciences
Notre Dame, IN 46556
Ph: 574-631-9438
Email: arocha1@nd.edu

Abstract:

Vegetation indices derived from solar and photosynthetically active radiation (PAR) sensors (i.e. radiation derived) have been under-utilized in inferring ecosystem function, despite measurement capability at hundreds of sites. This under-utilization may be attributed to reported mismatches among the seasonality of radiation- and satellite-derived vegetation indices and canopy photosynthesis; herein referred to as measurement biases. Here biases in radiation derived reflectance and vegetation indices were assessed using a decadal record of satellite and ground based spectroradiometer data, ecosystem phenology and CO_2 fluxes, and radiation derived vegetation indices (i.e. the Normalized Difference Vegetation Index [NDVI], the two band Enhanced Vegetation Index [EVI2]) from a high latitude tundra site (i.e. Imnaviat). At Imnaviat, we found poor correspondence between the three types of reflectance and vegetation indices, especially during the latter part of the growing season. Radiation derived vegetation indices resulted in incorrect estimates of phenological timing of up to a month and poor relationships with canopy photosynthesis (i.e. Gross Ecosystem Exchange (GEE)). These mismatches were attributed to solar position (i.e. solar zenith and azimuth angle) and a method, based on the diel visible and near-infrared albedo variation, was developed to improve the performance of the vegetation indices. The ability of radiation derived vegetation indices to infer GEE and phenological dates drastically improved once radiation derived vegetation indices were corrected for solar position associated biases at Imnaviat. Moreover, radiation derived vegetation indices became better aligned with MODerate resolution Imaging Spectroradiometer (MODIS) satellite estimates after solar position associated biases were corrected at Imnaviat and at 25 Fluxnet sites (~90 site years) across North America. Corrections developed here provide a way forward in

understanding daily ecosystem function or filling large gaps in eddy covariance data at a significant number of Fluxnet sites.

Keywords: Phenology, NDVI, EVI2, Solar Zenith, Gross Ecosystem Exchange, Arctic LTER

1.0 Introduction:

Vegetation indices, such as the Normalized Difference Vegetation Index (NDVI), have been used to infer ecosystem structure and function over the past half century (Rouse 1974). These indices utilize the low red reflectance -due to chlorophyll absorption-, and the high NIR reflectance -due to low absorption and high scattering- of green leaves to infer ecosystem function (e.g. leaf abundance, canopy physiology, and canopy phenology) (Gamon et al. 2010; Gamon et al. 2006). Historically, these indices were derived from satellite based reflectance; providing a proxy of ecosystem function at the global scale-albeit at low temporal resolution (e.g. monthly, bi-monthly). However, these indices also can be derived from commonly used up- and down-ward facing Photosynthetically Active Radiation (PAR) and solar radiation sensors (i.e. radiation derived); providing a low cost continuous measure of ecosystem function even when heavy cloud cover obscures satellite views of the surface (Huemmrich et al. 1999; Rocha and Shaver 2009; Wilson and Meyers 2007). Although radiation derived vegetation indices provide a powerful tool for understanding ecosystem function at sub-daily to annual timescales, a critical assessment of their uncertainties are surprisingly lacking.

Despite the wide use of PAR and solar radiation sensors across many eddy covariance sites, radiation derived vegetation indices have been under-utilized in inferring ecosystem function. Only a handful of studies have used radiation derived vegetation indices to infer ecosystem function, as compared to the thousands that have used satellite derived vegetation indices (Jenkins et al. 2007; Wohlfahrt et al. 2010; Wright and Rocha 2018). This imbalance may be due to the historical precedent of satellite data, or a lack of mechanistic understanding of measurement uncertainties in radiation derived indices. Radiation derived vegetation indices differ in magnitude and exhibit less seasonality than those derived from satellite data (Rocha and Shaver 2009). Jenkins et al. (2007) found that the slope of the relationship between radiation derived vegetation indices and canopy photosynthesis differed in the early and later part of the growing season. This contrasts with remote sensing work that models canopy photosynthesis from satellite derived vegetation indices with a single relationship across the season, and highlights a significant methodological knowledge gap (Sims et al. 2006; Sims et al. 2011; Xiao et al. 2005).

Although various hypotheses have been proposed to resolve the differences in radiation- and satellite- derived vegetation indices, the mechanisms are still debatable. The lack of correspondence between radiation- and satellite-derived vegetation indices have often been attributed to differences in the spatial scale of integration between the two measures or differences in sensor spectral resolution (Disney et al. 2004; Tittebrand 2009; Wang et al. 2004; Wang et al. 2012). Ground based radiation derived vegetation indices integrate a smaller area (i.e. ~100 x 100 m) than satellites such as the MODerate resolution Imaging Spectroradiometer (MODIS) (i.e. 100-1000 m) (Schmid 1997). Spatial mismatches are less likely to confound ground radiation- and satellite- derived reflectance and vegetation index comparisons in homogenous landscapes (Wittich and Kraft 2008). Radiation-derived vegetation indices also are very broad and integrate spectral information across the visible and infrared wavelengths, whereas satellite derived vegetation indices use more narrow spectral bands that focus on the red and NIR portions of the electromagnetic spectrum (Wittich and Kraft 2008). This spectral mismatch is more likely to influence the magnitude- but not the seasonality-of the vegetation indices (Elvidge and Chen 1995; Zhao et al. 2007). Although both these mechanisms are important at individual sites, they are unlikely to account for the inconsistency of radiation- and satellite-derived seasonality differences observed across many sites.

Sensor measurement biases have been largely overlooked when determining the causal mechanism behind differences in radiation- and satellite-derived vegetation indices (Balzarolo et al. 2011; Schaepman-Strub et al. 2006). Satellite sensors measure surface radiance, which are ultimately converted into a corrected surface reflectance that minimizes solar illumination and sensor view effects using a Bi-Directional Reflectance Function (BRDF) (Schaepman-Strub et al. 2006). The BRDF corrects for solar illumination effects from solar position to compare reflectance at the same view angle-typically defined at nadir. Such corrections are not made for radiation derived vegetation indices (Balzarolo et al. 2011; Huemmrich et al. 1999; Wilson and Meyers 2007). Although the radiation sensors are located above the canopy, these sensors integrate radiation from the entire hemisphere. Despite this hemispherical field of view, shortwave albedo has been shown to be sensitive to illumination angle (i.e. solar zenith and azimuth angles), which changes over the course of a day and year (Huemmrich et al. 1999). For example, broadband albedo measured with pyranometers have been shown to be dependent on solar zenith angle and illumination intensity for surfaces with high reflectivity such as snow (Carroll and Fitch 1981; Kriebel 1979; Wang et al. 2005; Wang and Zender 2010; Yang et al.

2008). However, little has been done to understand or correct the impact of illumination angle effects on radiation derived vegetation indices.

Here we assessed the ability of PAR and solar radiation derived reflectance proxies and vegetation indices to replicate MODIS satellite derived reflectance and vegetation indices; herein referred to as measurement biases. We also assessed the ability of PAR and solar radiation derived vegetation indices to infer ecosystem function (i.e. plant phenology and CO_2 fluxes). We focus on two commonly used vegetation indices: NDVI and EVI2 (Rocha and Shaver 2009). NDVI has more of a historical precedent in inferring ecosystem function, but EVI2 may provide a better proxy of ecosystem function due to its insensitivity to non-vegetated background reflectance (Jiang et al. 2008). Past remote sensing work has demonstrated the impact of solar position in influencing reflectance and vegetation indices, but lacked biological data to demonstrate the implications of ignoring such biases for inferring ecosystem function (Bhandari et al. 2011; Huete 1987; Ma et al. 2019; Middleton 1992). We hypothesized that solar position will lead to systematic biases in radiation derived vegetation indices that prevent these indices from correctly inferring vegetation phenology and seasonality in canopy photosynthesis at Imnaviat. We tested this hypothesis with a decadal record of PAR and solar radiation fluxes, MODIS, and ground based spectral radiometer measurements at a high latitude tundra site (Imnaviat), and further corroborated the patterns observed at Imnaviat with a synthesis of Fluxnet datasets. Imnaviat was chosen because of its landscape homogeneity, its rich long term ecological dataset (i.e. long term CO_2 fluxes and plant phenology), as well as its high latitude location with a frequently high solar zenith angle. The attributes of these data provide an ideal opportunity to determine the major sources of measurement biases leading to the discrepancy between satellite- and radiation-derived vegetation indices, and measures of seasonality in ecosystem function.

2.0 Methods

2.1 Site Description, Instrumentation, and Available Data

This study was conducted on a west-facing hillslope within the Imnaviat Creek watershed on the North Slope of Alaska, USA (68.61° N; 149.31° W). Vegetation at the site was characteristic of moist acidic tussock tundra with tussock cottongrass [*Eriophorum vaginatum*], dwarf birch [*Betula nana*], labrador tea [*Rhododendron tomentosum*], sphagnum moss [*Sphagnum spp.*], and scattered lichens covering the landscape (Euskirchen et al. 2012). The mean annual temperature at the site was -7 °C and the mean annual precipitation was 318 mm, with 40% occurring as rain and 60% as snow. Mean growing season (June-August) temperature was 6 °C, while mean non-growing season temperature was -11 °C.

In July of 2008, Imnaviat was instrumented with three (1 upward and two downward) CMP3 pyranometers that measured shortwave solar radiation (SW: units: W m^{-2}) [CMP3; Kipp and Zonen], three PAR sensors that measured Photosynthetically Active Radiation (PAR: units: µmol m^{-2} s^{-1}) [LI-190SA; Li-Cor, Lincoln NB], two downward looking surface temperature radiometers [IRT Infrared Thermometer; Apogee Instruments], a HMP temperature and humidity sensor [HMP45C-L; Campbell Scientific], and two TCAV soil temperature sensors [TCAV-L; Campbell Scientific]. Meteorological sensors were mounted at a height of 2.5 meters. Radiation sensors were well maintained, frequently leveled, and sent for factory calibration every 2-3 years during the measurement period. The radiation tower ran nearly continuously from July 2008-2018, and was powered by a battery bank connected to two solar panels, which were situated away from the direct field of view of the sensors.

The radiation tower was located ~300 m away from three Arctic Observatory Network (AON) flux towers located along the same west facing hillslope gradient (Euskirchen et al. 2012). The flux towers measured the Net Ecosystem Exchange of CO_2 (NEE) via the eddy covariance method, and a suite of meteorological variables including incoming and outgoing PAR and solar radiation, air temperature, humidity, wind speed, soil moisture, soil temperature, and snow depth (Baldocchi 2003). We analyzed the mean seasonal cycle of the daily Gross Ecosystem Exchange (GEE) at the mid-slope Moist Acidic Tundra (MAT) site from 2008-2018 to determine the relationship between vegetation indices and the seasonality of photosynthesis. The mid-slope MAT flux tower was chosen because of its similar vegetation composition, slope position, and NDVI seasonality to the nearby radiation tower [MAT Flux Tower NDVI vs. Imnaviat Radiation Tower NDVI R^2: 0.97; Slope: 1.01; Mean Absolute Error (MAE): 0.01]. AON data were obtained online at http://aon.iab.uaf.edu.

NEE flux partitioning was described in detail in Euskirchen et al. (2012, 2017), and followed standard Fluxnet protocols for partitioning NEE into canopy photosynthesis (Gross Ecosystem Exchange: GEE) and ecosystem respiration (ER). Briefly, NEE flux partitioning was accomplished by fitting a Q10 air temperature response function to well mixed (u-star> 0.10 s m^{-1}) NEE's that occurred during low light conditions (PAR< 50 µmol m^{-2} s^{-1}) (Ueyama et al. 2013; Euskirchen et al. 2017)). The basal respiration and Q10 parameters of the exponential model were determined through least squares fitting with “low light” NEE and air temperature data from a 30 day daily moving window. This empirically derived Q10 air temperature response function was used to estimate half hourly ER. Half hourly GEE was inferred from NEE by subtracting ER from NEE (GEE=NEE-ER), and temporally scaled up with daily summations.

2.2 Ground based Spectral Reflectance Measurements

Ground based reflectance was measured within the footprint of the Imnaviat radiation tower using three different spectroradiometers over the years. Spectral reflectance was measured with a Unispec (UniSpec-SC, PP-Systems, Amesbury, MA; Spectral Range: 300-1200 nm at 2 nm resolution) from 2008-2009, a dual channel Unispec (Unispec-DC, PP-Systems, Amesbury, MA; Spectral Range: 300-1200 nm at 2 nm resolution) from 2010-2012, and a FieldSpec 4 (Analytical Spectral Devices (ASD); Malvern Panalytical Ltd; United Kingdom; Spectral Range: 200-2400 nm at 2 nm resolution) from 2013-2018. Four ~100 m transects separated by ~30 m were established on the North and South side of the radiation tower forming a 200x120m grid within the tower footprint. Spectral reflectance was measured during midday hours (11:00 am-2:00 pm AST) every ~3 meters along each of the four 100 m transects either weekly, bi-monthly, or monthly during the growing season (June-August) of each year (n=240 scans per sampling date). A total of 62 sampling campaigns were undertaken from July 2008 to August 2018 with each campaign taking ~1 hour to accomplish.

Surface reflectance measurements followed standard procedures described in the spectroradiometer user manuals. Prior to measurements, each instrument was allowed a 15-20 minute warm up period. A freshly cleaned white Spectralon® diffuse reflectance panel

(Labsphere; North Sutton, NH) was used as a reflectance standard to convert spectroradiometer derived radiance into surface reflectance. Dark current measurements were taken by closing the detector "door", which prevented light from hitting the detectors and minimized measurement artifacts from background electrical instrument noise. Optimal measurement integration times were dependent on illumination conditions and were automatically determined by each sensor. White panel, dark current, and optimal measurement integration time measurements were taken frequently (i.e. every 3-5 minutes depending on sky conditions) to ensure high quality reflectance data. After each sampling campaign, surface reflectance data were quality checked for anomalous spectra (i.e. spectra that were >3 standard deviations from the mean) and averaged across all scans. These spectra were used to calculate NDVI and EVI2 using Equations [2] and [3] below and spectrally averaged MODIS wavelength and sensor response definitions for red- (MODIS spectral response weighted average of 620-670 nm) and NIR- reflectance (MODIS spectral response weighted average of 841-876 nm) (Xiong et al. 2006; Schaaf et al. 2002). We also spectrally averaged all wavelengths to calculate total and visible reflectance to derive a broad band visible, NIR (using equation 1), NDVI and EVI2 based on ASD spectroradiometer data. ASD averaged total reflectance was within 10% of the shortwave albedo, while ASD averaged visible reflectance was within 5% of PAR albedo measured by radiation sensors at Imnaviat.

2.3 Ground based Phenology

Individual plant species phenologies were measured from 2008-2018 in moist acidic tundra at the Toolik Lake Arctic Long Term Ecological Research (LTER) station. Toolik field station was situated ~7 km away and experienced similar weather to Imnaviat. A variety of phenological events (i.e. first snow free, first visible leaf, first leaf drop, first color change, and last leaf drop) were measured in several plots around Toolik lake in each year for the dominant MAT species (i.e. *Andromeda polifolia, Betula nana, Carex bigelowii, Cassiope tetragona, Empetrum nigrum, Eriophorum vaginatum, Ledum palustre, Polygonum bistorta, Rubus chamaemorus, Salix pulchra, Vaccinium uliginosum, Vaccinium vitis-idaea*). These phenological data were used to validate satellite- and radiation- derived NDVI and EVI2 estimates of the start-, end-, and length- of the growing season. The average of the first visible leaf for all species served as a proxy for the start of the growing season, whereas the maximum last leaf color change served as a proxy for the end of the growing season.

2.4 Radiation derived Vegetation Indices

The radiation tower at Imnaviat measured surface albedo in the visible (400-700 nm) and total shortwave wavelengths (300-2400 nm) of light. These albedo measures served as a proxy for red and near infrared reflectance (Rocha and Shaver 2009). Visible (α_V) albedo was calculated as the ratio between reflected ($_r$) and incoming ($_i$) PAR $\alpha_V = PAR_r/PAR_i$, while total albedo (α_T) was calculated as the ratio between reflected and incoming shortwave radiation [SW_r & SW_i, respectively] $\alpha_T = SW_r/SW_i$. α_V was used as a proxy for red reflectance, while both α_V and α_T were used in Equation 1 as a proxy for NIR reflectance (α_N) (Jenkins et al. 2007).

$$\alpha_N = W * \alpha_T - \alpha_V \quad \textbf{Equation [1]}$$

W in Equation 1 equaled 2 for all vegetation types, and represented a weighting term to separate α_N from α_V and α_T. Derivations of red and near infrared reflectance from ground based radiometers represented broadband definitions of narrowband quantities. α_N included dynamics in the near- and short-wave infrared region of the reflectance spectrum, while α_V included dynamics in the red, blue and green regions of the reflectance spectrum. Other ground radiometer derivations of α_N utilize similar assumptions (see Huemmrich et al., 1999 & Wilson and Meyers, 2007). We used Jenkins et al. (2007) derivation because of its parsimony and its high correlation with other α_N derivations (Jenkins vs. Huemmrich R^2 [Mean Absolute Error: MAE]: 0.91 [0.015]/ MAE Jenkins vs. Wilson & Meyers R^2 [MAE]: 0.99 [0.014]) for the sites used in this study. We also found that the conclusions from our analyses were independent of the different formulations of α_N.

We focused our analyses on the active growing season during snow-free periods. Data influenced by snow covered ground were identified with an albedo threshold of >0.3 (i.e. vegetation albedo <0.25 at all sites) and removed from the half hourly radiation datasets. Incoming and reflected radiation were averaged over the course of a day (i.e. n=48 for each value) to minimize diel solar zenith effects (Huemmrich et al. 1999; Rocha and Shaver 2009; Wilson and Meyers 2007). Sensor drift and snow and dirt accumulation on the sensors were identified as periods where PAR_i/SW_i fell beyond or below the mean plus or minus 2 standard deviations and subsequently removed. The final “cleaned” dataset contained daily ground radiometer values that were compared with MODIS reflectance and vegetation indices.

NDVI and EVI2 were calculated from radiation-, spectroradiometer- and MODIS-derived measures of near infrared (α_N) and red reflectance (α_R) with Equations [2] and [3] (Jiang et al. 2008).

$$NDVI = \frac{\alpha_N - \alpha_R}{\alpha_N + \alpha_R}$$ **Equation [2]**

$$EVI2 = 2.5\frac{\alpha_N - \alpha_R}{\alpha_N + 2.4\alpha_R + 1}$$ **Equation [3]**

2.5 Fluxnet Data Synthesis

We conducted a broader survey of ground based radiation derived vegetation indices with Fluxnet data to determine whether biases observed at the Imnaviat site were consistent across other sites (Table 1). Data from the Fluxnet network consisted of 25 sites and 90 site years of half hourly incoming ($_i$) and reflected ($_r$) PAR and shortwave data (Table 1). 12% of the sites were from crops, 8% were from deciduous forests, 25% were from evergreen forests, 28% were from grasslands, 20% were from arctic tundra, and 8% were from a shrub and grassland mix. Sites had a minimum of two years of data with a maximum of 6 years at 2 sites, and an average of 3.5 years for the entire dataset. PAR within the 400-700 nm spectral region was measured with a LI190 quantum sensor (LI-COR Inc., Lincoln, Nebraska) at 85% of the sites, while the remaining sites used either an Apogee quantum sensor (Apogee Instruments, Logan, Utah) or BF3 sunshine sensor (Dynamax, Houston Texas). Shortwave radiation (SW) within the 300-2800 nm spectral region was measured with a CM3 (Kipp & Zonen, Bohemia, NY) at 90% of the sites, while the remaining sites used an Apogee pyranometer (Apogee Instruments, Logan, Utah) or LI200 pyranometer (LI-COR Inc., Lincoln, Nebraska). Data were aligned with MODIS satellite data (see section 2.7) through 16- day averages that were centered on the MODIS composite date.

2.6 Testing and Correcting for Solar Position Biases

We corrected solar position biases using diel relationships between solar position and albedo throughout the season. Diel NIR and visible albedo variability can be more than twice as large as observed over the course of a season (Huemmrich 1999). These large diel visible and NIR albedo variations cannot be representing changes in canopy leaf area, that are often related to vegetation indices, because LAI changes over much longer time scales than a day (i.e. days to weeks)(Stoy 2013). Rather, this large diel variation arises from the anisotropic properties of surface reflectance (i.e. the bidirectional reflectance distribution function) and possibly other sensor issues, such as a sensors' cosine response function (Huete 1987; Middleton 1992; Rahman et al. 1993).

Here we used the diel variation in albedo and solar position to empirically derive a correction factor to apply over the course of the season. Solar position was calculated for each site and half hour using the site latitude and longitude and time of year (Myers 2017). We removed divided each daily averaged visible and NIR albedo into each half hourly visible and NIR albedo value to remove vegetation phenology effects and focus solely on sub-daily variations associated with solar position (Equation 4).

$$\alpha_{Cor} = \frac{Daily\ "unbiased"\ Value}{Half\ Hourly\ "biased"\ Value} = \frac{\alpha_d}{\alpha_h} \qquad \textbf{Equation [4]}$$

Here, given the large sub-daily variation in solar position, we assumed that the half hourly NIR and visible albedos were more “biased” in response to solar position than the daily averaged values (i.e. “unbiased). Hence, α_{Cor} represented a correction factor that could be used to remove the solar position bias from the albedo measurements. For each day, we calculated 48 half hourly α_{Cor} ratios, which could be used to create a temporally consistent albedo value throughout the day through multiplication (i.e. Half Hourly biased *Daily average unbiased/ Half Hourly biased = Daily averaged unbiased). This sub-daily consistency of NIR and visible albedos were more aligned with the fact that LAI changes occur over longer time scales than a day. By understanding the dependence of α_{Cor} on solar position, we could remove any measurement bias introduced by seasonal changes in solar zenith and azimuth. If radiation derived albedos were not dependent on solar position, then α_{Cor} would equal one across different solar azimuth and zenith angles. If radiation derived albedos were dependent on solar position, then α_{Cor} would significantly differ from 1 and scale with solar azimuth and zenith angles.

Here we used the solar position dependence of α_{Cor} at the half hourly time scale to reduce any solar position biases observed across the season. Half hourly α_{Cor} was empirically related to half hourly solar-zenith and -azimuth angles through a machine learning squared exponential Gaussian process regression model. This half hourly statistical model was used to predict α_{Cor} across the season using daily averaged solar zenith and azimuth angles as dependent variables. Regression model predicted daily α_{Cor} was multiplied by the daily averaged visible and NIR albedos to produce solar position (i.e. “biased free”) corrected α_V and α_N. Solar position corrected α_V and α_N were then used to recalculate NDVI and EVI2 using Equations 2 and 3.

Analyses were accomplished with Matlab's Regression Learner application (MATLAB 2019b; Mathworks Inc. Natick, MA).

2.7 MODIS Data

We compared MODIS reflectance and vegetation indices to radiation derived proxies and measures. For the Fluxnet data synthesis, MODIS Nadir-BRDF adjusted 500 m resolution collection 4 surface reflectance data (MODIS NBAR; MCD43A) were extracted from a 2.5 x 2.5 km^2 area centered at each tower location in 2012 (http://daac.ornl.gov) (Schaaf et al. 2002; ORNL DAAC 2018). We also used the equations from Liang (2000) to calculate a total and visible albedo from the seven MODIS spectral bands. These MODIS derived total and visible albedos were used to derive broadband vegetation indices following Equations 1-3. For Imnaviat, we used collection 6 version 1 daily Nadir BRDF-Adjusted reflectance (MCD43A4) and extracted data at various spatial scales (i.e. 0.25, 6.25, 20.25, 210.25, and 420.25 km^2) to determine the impact of spatial aggregation on the comparison between ground and satellite based data (Shuai et al. 2013). Data with >80% of pixels passing quality control were used in the analyses. Only growing season MODIS data, as defined by ground based snowless terrestrial albedo values greater than 0.25, were used in the analyses.

2.8 Phenology Model

The start, end, and length of the growing season was determined with a phenology model fit to the observed seasonal cycle of MODIS- and radiation- derived NDVI and EVI2 in each year at Imnaviat. The phenology model was a double-logistic function that predicted each vegetation index based on the day of year (t) (Beck et al. 2006; Fisher et al. 2006; Fisher et al. 2007) (Equation 5):

$$v(t) = v_{min} + v_{amp}\left(\frac{1}{1+e^{m_1 - n_1 t}} - \frac{1}{1+e^{m_2 - n_2 t}}\right) \qquad \textbf{Equation [5]}$$

The model was fit by minimizing the sum of squared residuals between model predictions and observed values. The fitted parameters of the model were v_{min} and v_{amp}, m_1, n_1, m_2, and n_2. v_{min} and v_{amp} were related to the minimum and amplitude values of the spectral index, respectively. The parameters in the two exponents determined the seasonality with m_1 and n_1 related to the rate and timing of green-up, and m_2 and n_2 related to the rate and timing of senescence. The start of the growing season was given by $t = m_1/n_1$, the end of the growing season was given by $t = m_2/n_2$, and the length of the growing season was determined by the difference between the start and end of the growing season.

2.9 Statistical Analyses:

Statistical analyses included least squares linear regression to determine the relationship between two variables, and Mean Absolute Error (MAE) to determine the prediction error of a model or the error associated with the comparison of a set of similar observations (Ramsey 2013). Statistical significance was determined at the 95% confidence level.

3. Results

3.1 Assessing Spatial Aggregation Biases

The scale of spatial integration had little impact on the comparison between tower and MODIS based vegetation indices indicating landscape coherence in phenology within the region surrounding Imnaviat (Figure 1). Here we minimized spectral definition differences among sensors by comparing spectroradiometer- and MODIS- derived reflectance's and vegetation indices. Spectroradiometer derived NDVI explained 70% of the variability in MODIS derived NDVI, whereas spectroradiometer derived EVI2 explained 60% of the variability in MODIS derived EVI2. The MAE increased slightly from 6% of NDVI at the ecosystem/watershed level (0-10 km^2) to 7% of NDVI at the regional scale (>300 km^2). EVI2 exhibited greater sensitivity to spatial integration with MAEs increasing from 14% of EVI2 at the ecosystem/watershed scale to 20% of EVI2 at the regional scale.

3.2 MODIS- vs. radiation-derived reflectance and indices comparison

In general, spectroradiometer- and MODIS- derived reflectances and vegetation indices were more related to each other than those derived from radiation fluxes at Imnaviat (Table 2). Vegetation indices yielded higher correlations among measurement types than did red and NIR reflectance. For example, reflectance R^2's ranged from 0.17-0.22 for NIR and red reflectance, while vegetation index R^2's ranged from 0.34 to 0.67. Correlations among radiation-, spectroradiometer-, and MODIS-derived measures were typically higher for EVI2 than for NDVI. The poor relationships between radiation- and MODIS/spectroradiometer- derived vegetation indices were largely attributed to differences in seasonality among the MODIS/spectroradiometer- and radiation- derived measures.

Seasonality differed among radiation-, spectroradiometer-, and MODIS derived- reflectance and vegetation indices at Imnaviat (Figure 2). Correspondence among the three measures was greatest for red reflectance and smallest for NIR, NDVI, and EVI2. Red reflectance demonstrated similar seasonality among the measures with higher reflectance in the shoulder seasons and minimum values during the peak of the growing season. In contrast, NIR reflectance, NDVI, and EVI2 were low at the start of the growing season, reached a maximum during peak growing season, and then declined to a minimum at the end of the growing season. All three measures of NIR, NDVI and EVI2 exhibited similar seasonality up until the peak of the growing season, but differed towards the end of the growing season. Radiation-derived NIR reflectance and vegetation indices were larger than MODIS and spectroradiometer- derived quantities towards the latter part of the growing season. Consequently, differences between MODIS and spectroradiometer- and radiation-derived NIR, NDVI, and EVI2 exhibited strong seasonality with the largest mismatch towards the second half of the growing season.

3.3 Assessing Sensor Biases

Seasonal differences between MODIS- and radiation- derived indices observed in Figure 2 were correlated with solar zenith angle at Imnaviat (Figure 3). Larger solar zenith angles produced larger differences between MODIS- and radiation- derived NIR, NDVI, and EVI2, but had no impact on differences between MODIS- and radiation- derived red reflectance. Solar zenith angle explained 41% of the variability in NIR reflectance biases, 28% of the variability in NDVI biases, and 45% of the variability in EVI2 biases. This represented a bias of 0.004 per 1° change in zenith angle for NIR reflectance, and a bias of 0.006 per 1° change in zenith angle for NDVI and EVI2.

The relationship between measurement bias and solar zenith angle at Imnaviat were consistent across Fluxnet sites located in vastly different biomes (Figure 4). However, in contrast to the observed solar zenith dependent measurement biases at the Imnaviat site, there was a statistically significant measurement bias dependence on solar zenith angle at some of the Fluxnet sites for red reflectance. For the Fluxnet dataset, MODIS and radiation derived NIR differences positively scaled with solar zenith angle and all biomes exhibited similar slopes that ranged from 0.002 to 0.003 per 1^{o} change in zenith angle. The solar zenith dependent biases in NIR and red reflectance carried over to NDVI and EVI2, but sometimes canceled each other out. This cancelling out effect was more predominant for NDVI than for EVI2. For example, NDVI biases were unrelated to solar zenith angle for evergreens and grass shrublands, whereas solar zenith angle was correlated with EVI2 biases in all biomes. The bias sensitivity to solar zenith angle ranged from 0.001 to 0.005- for NDVI, and from 0.003 to 0.005- per 1^{o} change in zenith angle for EVI2.

3.4 Assessing Bandwidth Biases

We used the full range spectroradiometer ASD data (300-2400 nm) to determine whether the measurement bias dependence on solar position was attributed to broadband versus narrowband definitions of red and near infrared reflectance used by the radiation sensors (Figure 5). Correlations between solar zenith angle and the difference between broadband and narrowband (i.e. Bandwidth Biases) definitions for red (p-value: 0.94), NDVI (p-value: 0.21), and EVI2 (p-value: 0.06) were not statistically significant. Bandwidth biases were marginally significant and related to solar zenith angle for NIR (p-value: 0.04), but were opposite in sign to the expected relationships observed in Figures 3 & 4. Moreover, solar zenith angle only explained 10% of the variation in bandwidth biases, as opposed to the 67% of the variation in radiation tower and MODIS differences explained by zenith angle in Figure 3.

Similar results were found across the Fluxnet sites using MODIS data and differencing broad- and narrow- band vegetation indices (Figure 1S; Table 1S). Although many relationships were statistically significant, solar zenith angle only explained <10% of the variation in bandwidth biases for NDVI, and <11% of the variation in bandwidth biases for EVI2 across all Fluxnets sites on average (Supplementary Figure 1). Moreover, the bandwidth bias sensitivity to solar zenith angle was sometimes the opposite sign of the expected positive relationships in Figures 3 and 4 and were on average one to two orders of magnitude lower than that observed for tower and MODIS differences for red, NIR, NDVI, and EVI2 (Supplementary Table 1).

3.5 Correcting Solar Position Biases

Diel variability in solar position affected radiation derived visible and NIR albedos that were used as red and NIR reflectance at Imnaviat (Figure 6). Over the growing season, daily averaged solar zenith angle changed by 19^{o}, while daily averaged solar azimuth angle changed by 7^{o} (Figure 6 inset). Visible and NIR albedo were more sensitive to solar zenith- than azimuth- angles as illustrated by the small scatter in Figure 6. NIR albedo was more sensitive to solar zenith angle than visible albedo and was almost two times higher than its expected value at an 80^{o} zenith angle. Consequently, the correction factor for NIR albedo declined markedly above 70^{o} from 0.85 to 0.59, whereas the correction factor for visible albedo changed by <1% above 70^{o} solar zenith angle.

Correcting solar position biases using the machine learning approach described in section 2.6 improved the agreement between MODIS- and radiation- derived red and NIR reflectance, NDVI, and EVI2 at Imnaviat (Figure 7). After correcting for the dependence of measurement biases on solar position, MAE decreased and R^2 increased between MODIS- and radiation-derived reflectance and vegetation indices (Table 3; Figure 7). An exception to this occurred for MODIS red reflectance, where the R^2 and MAE did not significantly change after correction due to its low sensitivity to solar position. MAE decreased by 40% for NDVI and EVI2, and by 33% for NIR reflectance after applying the correction factor for seasonal changes in solar position.

Correcting solar position biases using the machine learning approach also improved the agreement between MODIS- and radiation-derived NDVI and EVI2 across the Fluxnet sites (Figure 8). Correcting for measurement biases introduced by solar position reduced the MAE between MODIS- and radiation- derived NDVI and EVI by 5% to 77%. Grasslands and tundra experienced the largest decrease in MAE, while crops experienced the smallest decreases in MAE once the impact of solar position on radiation derived albedo and vegetation indices were corrected. There was quite a bit of variability in the improved correspondence between MODIS- and radiation-derived vegetation indices among sites. However, it was difficult, if not impossible, to attribute this variability to underlying environmental, biophysical or site specific factors without additional site and sensor specific information. Regardless, correcting biases in vegetation indices for solar position improved the correspondence between MODIS- and radiation- derived vegetation indices at 85% of the sites investigated.

3.6 Implications for Inferring Ecosystem Function with radiation derived NDVI and EVI2

Biases associated with solar position confounded the ecophysiological interpretation of radiation derived NDVI and EVI2 at Imnaviat (Figure 9). Uncorrected radiation derived vegetation indices exhibited hysteretic relationships with GEE with different sensitivities-as measured by the slope of the line- in the first and second half of the growing season. GEE was lower for the same value of NDVI/EVI2 in the first part of the growing season, and higher for the same value of NDVI/EVI2 in the second part of the growing season. The relationship between NDVI/EVI2 became more linearized with a single relationship throughout the growing season once vegetation indices were corrected for their solar position dependence (Figure 9 solid line). Uncorrected NDVI explained 37% of the variability in GEE, whereas solar position corrected NDVI explained 85% of the variability in GEE. Similar patterns were found for EVI2. Uncorrected EVI2 explained 37% of the variability in GEE, whereas solar position corrected EVI2 explained 89% of the variability in GEE.

Solar position also confounded the determination of the start, end, and length of the growing season at Imnaviat (Figure 10). On average, correcting radiation derived vegetation indices for solar position decreased the MAE between leaf level measures of phenology up to ~10 days. Differences between corrected and uncorrected NDVI/EVI2 derived phenologies were greatest for the length of the growing season due to compounding errors associated with the start and end of the growing season estimates. Uncorrected NDVI/EVI2 demonstrated reduced skill at determining the end of the growing season relative to the start; a finding that is consistent with trends observed in Figure 2. Solar position corrected radiation derived NDVI/EVI2 performed similarly to-or in some cases-better than MODIS in predicting the start and end of the growing season, especially for EVI2. For example, solar position corrected radiation derived EVI2 performed better than MODIS EVI2 in predicting the start and length of the growing season. When MODIS- and radiation- derived phenological predictions were combined, NDVI outperformed EVI2 by 5 days for the start of the growing season and 7 days for the length of the growing season, whereas EVI2 outperformed NDVI by 1 day for the end of the growing season.

4.0 Discussion:

Solar position introduced significant bias on PAR and solar radiation derived vegetation indices, especially during the latter part of the growing season. These errors were largely independent of broad- to narrow-band definitions (Figures 5 & 1S; Table 1S), and sensor spatial aggregation errors associated with landscape heterogeneity (Figure 1). The effect of satellite spatial aggregation errors was minimized by focusing on a relatively homogenous site (i.e. Imnaviat), and were much smaller than that observed for measurement biases [i.e. <0.02 change in vegetation index MAE from 0-400 km^2 (Figure 1) compared to ~0.05 MAE for tower and MODIS vegetation comparisons (Table 2)] (Wang et al. 2012). Measurement biases also were universal and occurred across a wide variety of latitudes, biomes, and sites indicating a persistent error that cannot be explained by individual site specific conditions (Figures 3,4,7,8). These measurement biases accounted for some of the limitations and issues highlighted in previous work with radiation derived vegetation indices (Jenkins et al. 2007; Rocha and Shaver 2009; Wang et al. 2004; Wittich and Kraft 2008). To our knowledge, this is the first paper, since Huemmrich et al.'s (1999) seminal work, to develop a methodology using the diel variation in albedo to correct for these biases and improve the performance of these indices in inferring ecosystem function.

Historically, solar position biases on radiation- derived albedo and vegetation indices were assumed to be negligible over the course of a season, despite known diel variation (Huemmrich et al. 1999). This incorrect assumption was likely due to data limitations from looking at a single site over a short time period, the exclusion of solar azimuthal effects, and a lack of multi-sensor comparisons. Unlike past work, our conclusions were supported by multiple independent physical and ecological observations. First, solar position corrections improved correspondence between satellite- and radiation- derived vegetation indices at Imnaviat and Fluxnet sites (Figures 7 and 8; Table 3). Second, solar position corrections improved the ability of radiation derived vegetation indices in capturing phenological timing and C fluxes (Figures 9 and 10). It is clear that our use of combining long time series data obtained from different sensors and scales was essential in validating and assessing measurement biases in radiation derived vegetation indices. Our results also demonstrated that, in some cases, solar position associated NIR and visible biases canceled each other out in the calculation of the vegetation index. This cancelation effect may explain the discrepancy between this study and past work at single sites that assumed negligible solar position biases.

Addressing solar position biases in visible and NIR albedo are important because these biases resulted in poor relationships with MODIS data and poor inferences of ecosystem function. Without correcting for solar position, measurement biases reduced the explained variation in canopy photosynthesis and increased estimation error of the start, end, and length of the growing season (Figures 9,10). Radiation derived vegetation indices also exhibited less seasonality than MODIS, which was consistent with previous work with higher than expected NIR and vegetation indices towards the latter part of the growing season (Rocha and Shaver 2009; Wittich and Kraft 2008). These unique attributes of radiation derived vegetation indices have been previously reported, but often incorrectly attributed to bandwidth biases rather than solar position (Rocha and Shaver 2009; Jenkins et al. 2007; Wang et al. 2004). Broadband derivations of red and NIR reflectance incorporate dynamics in the shortwave infrared that could potentially confound the seasonality of the broadband red, NIR, NDVI, and EVI2 measured by PAR and shortwave radiation sensors. However, bandwidth errors exhibited weak to non-existent relationships with solar position for broadband radiation derived indices across Imnaviat and the Fluxnet sites (Figures 5 and 1S; Table 1S). On the other hand, measurement bias sensitivity to solar zenith angle was an order of magnitude larger than that observed for broadband biases across both Imnaviat and Fluxnet sites (Figures 5; Figure 1S; Table 2S). The improved ability of radiation derived vegetation indices to replicate MODIS narrowband reflectance and VIs once solar position correction was applied provides strong evidence to attribute radiation derived biases to solar position, rather than bandwidth errors (Figures 7,8, 1S).

Here we used a simple machine learning empirically based model based on actual half hourly data to correct the seasonal biases in visible and NIR albedo. Our empirical model had high predictive power, explaining 85-95% of solar position biases, followed an expected BRDF response (i.e. a non-linear positive response with solar zenith angle), and included additional factors that may be difficult to parameterize in a BRDF model (Figure 6). For example, radiation sensors may have internal measurement biases due to solar position, known as a sensors cosine response (Blonquist et al. 2009; Ross and Sulev 2000). A sensor's cosine response describes how solar radiation is integrated across all solar zenith and azimuthal positions on a Lambertian receiver. This response differs among sensors and would be subject to measurement drift issues that would be difficult to quantify without additional information. Differences in a sensor's cosine response also may explain the differences in the sensitivity of radiation derived measurements to solar zenith angle among sites (Figures 4,8).

Quantifying and understanding measurement errors and limitations remains an important process in the scientific community (Kratzenberg et al. 2006; Richardson et al. 2008; Ross and Sulev 2000). This is especially true in ecosystem ecology as new, interdisciplinary, and automated remote- and near-sensing measurement techniques are being more commonly used. Understanding error sources and applying the proper corrections will result in improved understanding or quantification of ecosystem function. For example, the strong relationship between solar position corrected radiation derived vegetation indices and canopy photosynthesis demonstrate promise in using these data to fill long gaps in eddy covariance flux data. Moreover, the high correspondence between solar position corrected radiation- and satellite-derived vegetation indices indicates that these data can be valuable in gap filling MODIS data during cloudy periods (Figure 7). However, we caution future users of such data to also consider other potential important sources of measurement error, such as sensor drift and sensor spectral sensitivity, that may significantly alter the continuity of high quality radiation based vegetation indices (Kratzenberg et al. 2006; Ross and Sulev 2000). We encourage future work to implement, or improve upon, our methodology to gain further understanding the temporal dynamics of ecosystem C cycling and phenology with vegetation indices derived from solar and photosynthetically active radiation fluxes.

Acknowledgements

This work was supported by the National Science Foundation (NSF) grants #1065587 and #1026843 to the Marine Biological Laboratory, and NSF grants #1556772 to the University of Notre Dame. This work also was funded by the NSF division of Polar Programs Arctic Observatory Network grant numbers #856864, #1304271, #0632264, and #1107892. Any use of trade, product, or firm names is for descriptive purposes only and does not imply endorsement by the US Government.

Site Name	Latitude	Years	PFT	PAR Sensor	Pyranometer Sensor
Bondville[1]	40	2004-2007	Crop	Apogee	LI200
ARM SGP[1]	36.5	2004-2009	Crop	LI190	CM3
Sioux Falls[2]	43.2	2007-2009	Crop	NA	NA
UCI 1989[3]	55.9	2002-2005	Deciduous	LI190	CM3
UCI 1998[3]	56.5	2002-2005	Deciduous	LI190	CM3
Black Hills[4]	44.2	2004-2008	Evergreen	LI190	CM3
Flagstaff Managed[5]	35.1	2006-2009	Evergreen	BF3/LI190	CM3
UCI 1850[3]	55.9	2002-2005	Evergreen	LI190	CM3
UCI 1930[3]	55.9	2002-2005	Evergreen	LI190	CM3
UCI 1964[3]	55.9	2002-2005	Evergreen	LI190	CM3
UCI 1981[3]	55.9	2002-2005	Evergreen	LI190	CM3
Brookings[4]	44.3	2004-2010	Grassland	NA	NA
Canaan Valley[4]	39.1	2004-2010	Grassland	Apogee	CM3
Cottonwood[4]	43.9	2006-2009	Grassland	NA	NA
Flagstaff Wildfire[5]	35.4	2005-2009	Grassland	BF3/LI190	CM3
Fort Peck[4]	48.3	2002-2008	Grassland	LI190	Apogee
Goodwin Creek[4]	34.3	2002-2006	Grassland	Apogee	CM3
Kendall[6]	31.7	2004-2009	Grassland	NA	NA
Audubon[4]	31.8	2004-2009	Grassland	LI190	CM3
Ivotuk[7]	68.5	2004-2006	Tundra	LI190	CM3
Imnaviat[8]	68.6	2009-2011	Tundra	LI190	CM3
Unburned[9]	68.9	2008-2011	Tundra	LI190	CM3
Severe[9]	68.9	2008-2011	Tundra	LI190	CM3
Moderate[9]	68.9	2008-2011	Tundra	LI190	CM3
Santa Rita Mesquite[10]	31.8	2004-2007	Grassland/ Shrub	NA	NA

Table 1. Site names, location, years, Plant Functional Type (PFT) and sensors used at each of the sites used in this study. [1]Hollinger et al. (1994); [2]Verma et al. (2005); [3]Goulden et al. (2011); [4]Wilson and Myers (2007); [5]Dore et al. (2016); [6]Scott et al. (2010); [7]McEwing et al. (2015); [8]This study; [9]Rocha and Shaver (2011); [10]Scott et al. (2009)

	Spectroradiometer v. MODIS *R^2 [MAE]*	**Spectroradiometer v. Radiation** *R^2 [MAE]*	**MODIS v. Radiation** *R^2 [MAE]*
Red	0.22 [0.01]	0.21 [0.01]	0.19 [0.01]
NIR	0.17 [0.03]	0.20 [0.03]	0.22 [0.03]
EVI2	0.67 [0.03]	0.42 [0.09]	0.42 [0.05]
NDVI	0.55 [0.05]	0.34 [0.11]	0.34 [0.05]

Table 2. R-squared and Mean Absolute Error (MAE) of relationships among spectroradiometer-, MODIS-, uncorrected radiation- derived reflectance and vegetation indices.

	MODIS v. U-Radiation *R^2 [MAE]*	**MODIS v. C-Radiation** *R^2 [MAE]*
Red	0.19 [0.01]	0.19 [0.01]
NIR	0.22 [0.03]	0.47 [0.02]
EVI2	0.42 [0.05]	0.56 [0.03]
NDVI	0.34 [0.05]	0.56 [0.03]

Table 3. R-squared and Mean Absolute Error (MAE) of relationships among MODIS- , uncorrected (U) radiation-, and corrected (C) radiation- derived reflectance and vegetation indices.

Figure 1: Mean Absolute Error (MAE {unitless VI ratios}: blue circles left y-axis) and r-squared (R^2{unitless}: red triangles right y-axis) of the relationship between spectroradiometer- and MODIS- derived NDVI (top) and EVI2 (bottom) at different MODIS spatial integration scales at Imnaviat.

Figure 2: Seasonal cycle of spectroradiometer- (black diamonds), radiation- (blue dots), and MODIS-derived (red dots) red (A) and near-infrared (B) reflectances, and NDVI (C) and EVI2 (D) from quality controlled 2008-2018 Imnaviat data.

Figure 3: Dependence of MODIS- and radiation- derived differences on solar zenith angle for red reflectance (A), near infrared reflectance (B), NDVI (C), and EVI2 (D) at Imnaviat. Regression lines indicate significant relationships at the 95% confidence level.

Figure 4: Dependence of MODIS- and radiation- derived differences on solar zenith angle for red reflectance (A), near infrared reflectance (B), NDVI (C), and EVI2 (D) from Fluxnet sites across biome types. Lines in panels C and D are only for statistically significant relationships at the 95% confidence level.

Figure 5: Dependence of ground based spectroradiometer broad- and narrow-band derived differences (i.e. broadband-narrowband) on solar zenith angle for red reflectance (A), near infrared reflectance (B), NDVI (C), and EVI2 (D) at Imnaviat. Regression lines indicate significant relationships at the 95% confidence level.

Figure 6: The correction factor dependence on solar zenith angle for visible (solid dots) and near infrared (open dots) albedo. The inset plot shows seasonal changes in daily averaged solar zenith angle (solid line) and daily averaged azimuth angle (dotted line). The grey highlighted area denotes the growing season period at Imnaviat.

Figure 7: Correspondence between radiation- and MODIS- derived red (A) and near infrared (B) reflectances, and NDVI (C) and EVI2 (D) at Imnaviat. Grey dots are MODIS and uncorrected radiation derived reflectance and indices, whereas triangles are MODIS and radiation derived reflectance and indices that were corrected for solar position biases.

Figure 8: Average percent change in the Mean Absolute Error (MAE) between MODIS satellite- and radiation-derived NDVI (black bars) and EVI2 (grey bars) relative to the uncorrected values

at the Fluxnet sites. Fluxnet sites were grouped by ecosystem type, and error bars represent standard errors.

Figure 9: Relationship between Imnaviat Gross Ecosystem Exchange (GEE) and solar position corrected (open triangles) and uncorrected (grey circles) radiation derived vegetation indices. NDVI-GEE relationships are in left panel (A), whereas EVI2-GEE are in right panel (B). The solid line represents the correlation between the solar position corrected vegetation index and GEE, whereas the dotted line represents the correlation between uncorrected vegetation indices and GEE. Hatched arrows in left panel represent the hysteresis in the relationship between uncorrected NDVI and GEE, while numbers represent the day of year of each observation.

Figure 10: Mean Absolute Error (MAE) of the start-(SOS), length-(LOS), and end-(EOS) of the growing season derived from MODIS- (black bar), uncorrected radiation- (grey), and solar position corrected radiation- (dark grey) derived NDVI (A) and EVI2 (B) at Imnaviat.

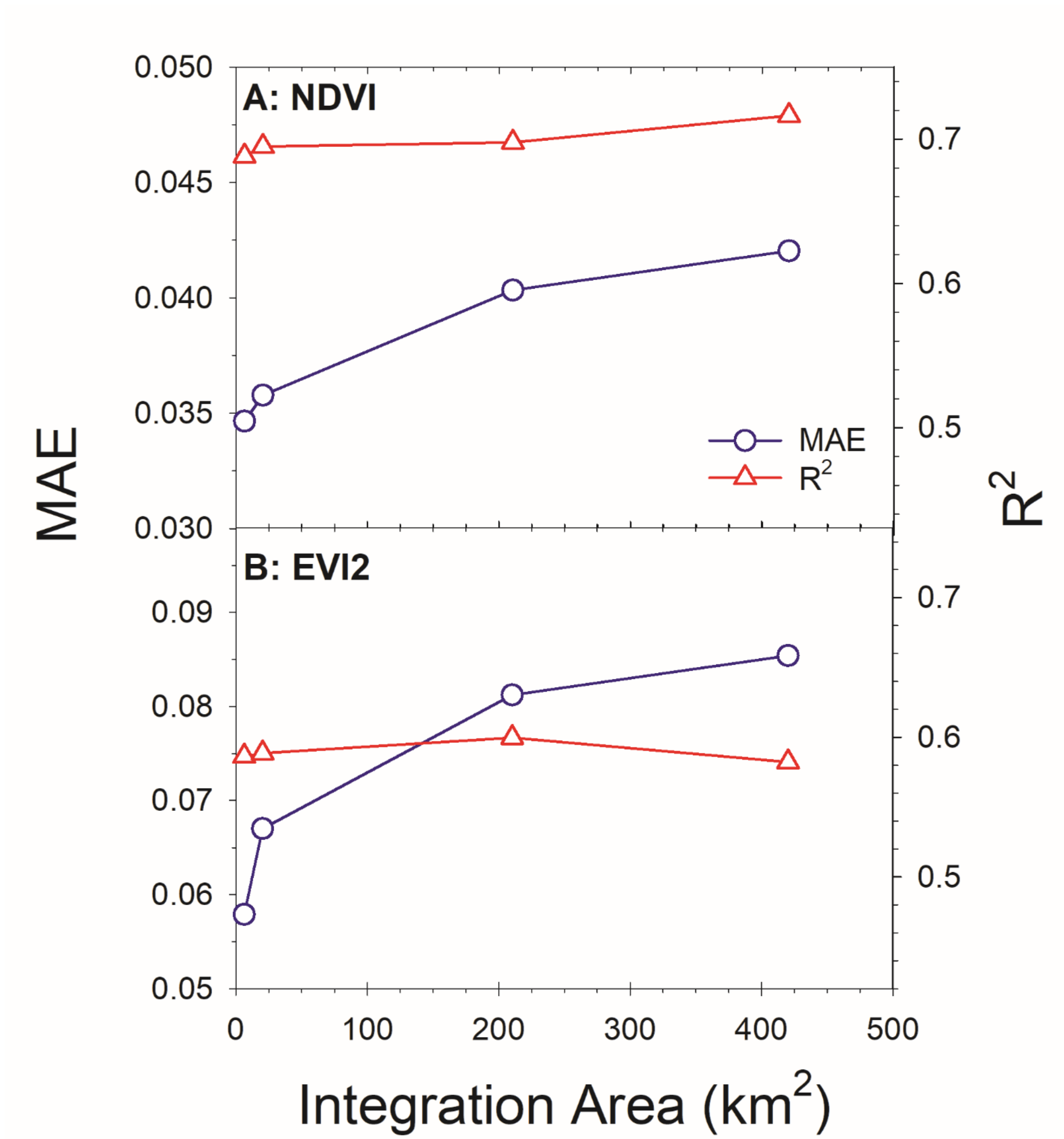
A: NDVI
B: EVI2
MAE
R^2
MAE
R^2
0.050
0.045
0.040
0.035
0.030
0.09
0.08
0.07
0.06
0.05
0.7
0.6
0.5
0.7
0.6
0.5
0
100
200
300
400
500
Integration Area (km^2)

Figure 1.

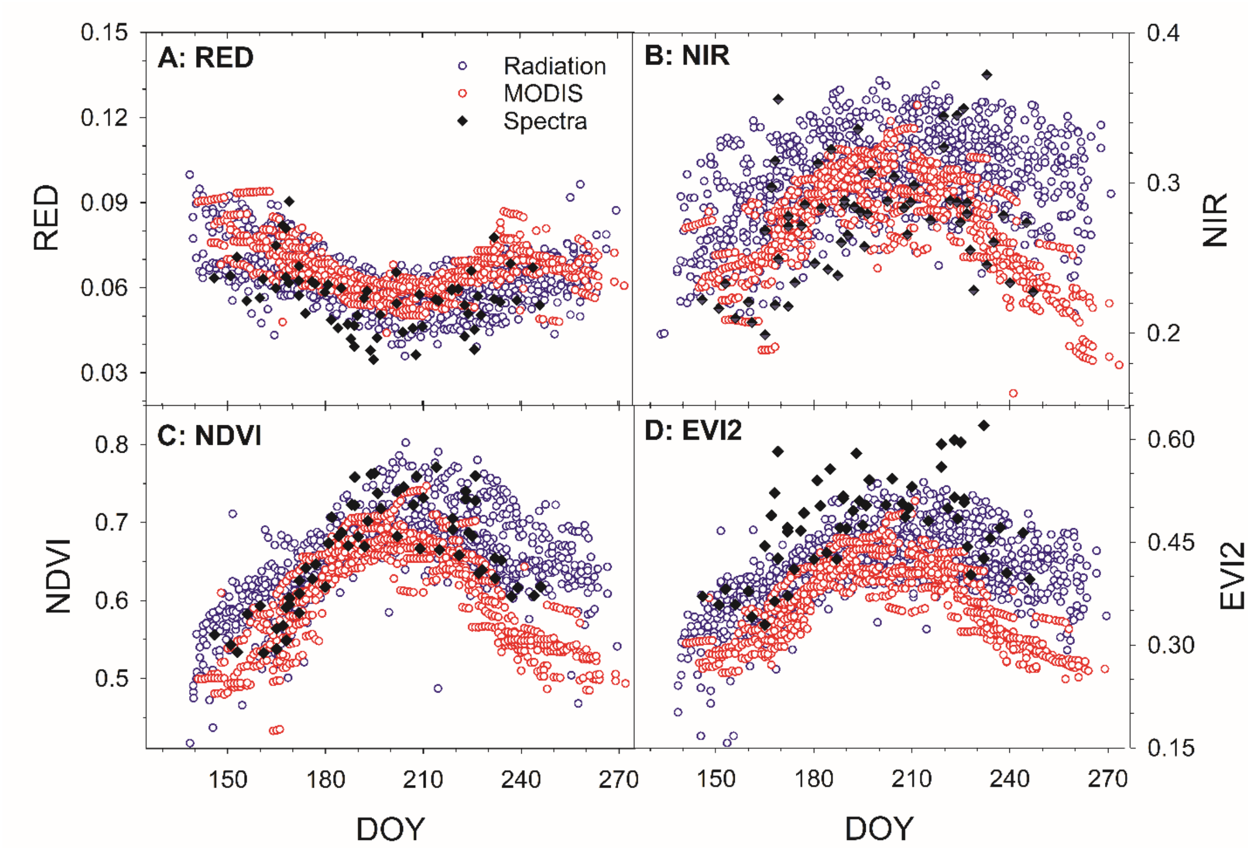
A: RED
B: NIR
C: NDVI
D: EVI2
Radiation
MODIS
Spectra
RED
NIR
NDVI
EVI2
0.15
0.12
0.09
0.06
0.03
0.4
0.3
0.2
0.8
0.7
0.6
0.5
0.60
0.45
0.30
0.15
150
180
210
240
270
DOY
DOY

Figure 2.

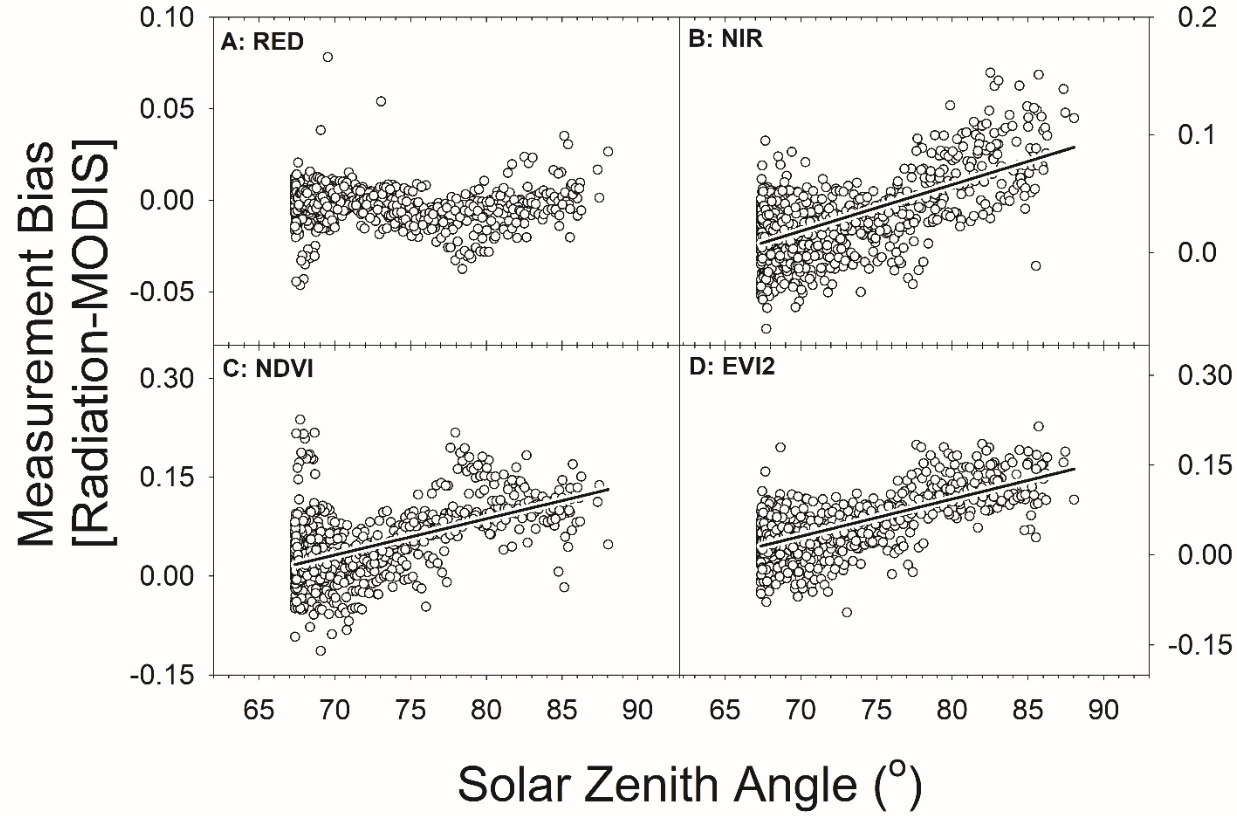
A: RED
B: NIR
C: NDVI
D: EVI2
Measurement Bias
[Radiation-MODIS]
Solar Zenith Angle (°)
0.10
0.05
0.00
-0.05
0.30
0.15
0.00
-0.15
0.2
0.1
0.0
0.30
0.15
0.00
-0.15
65
70
75
80
85
90

Figure 3.

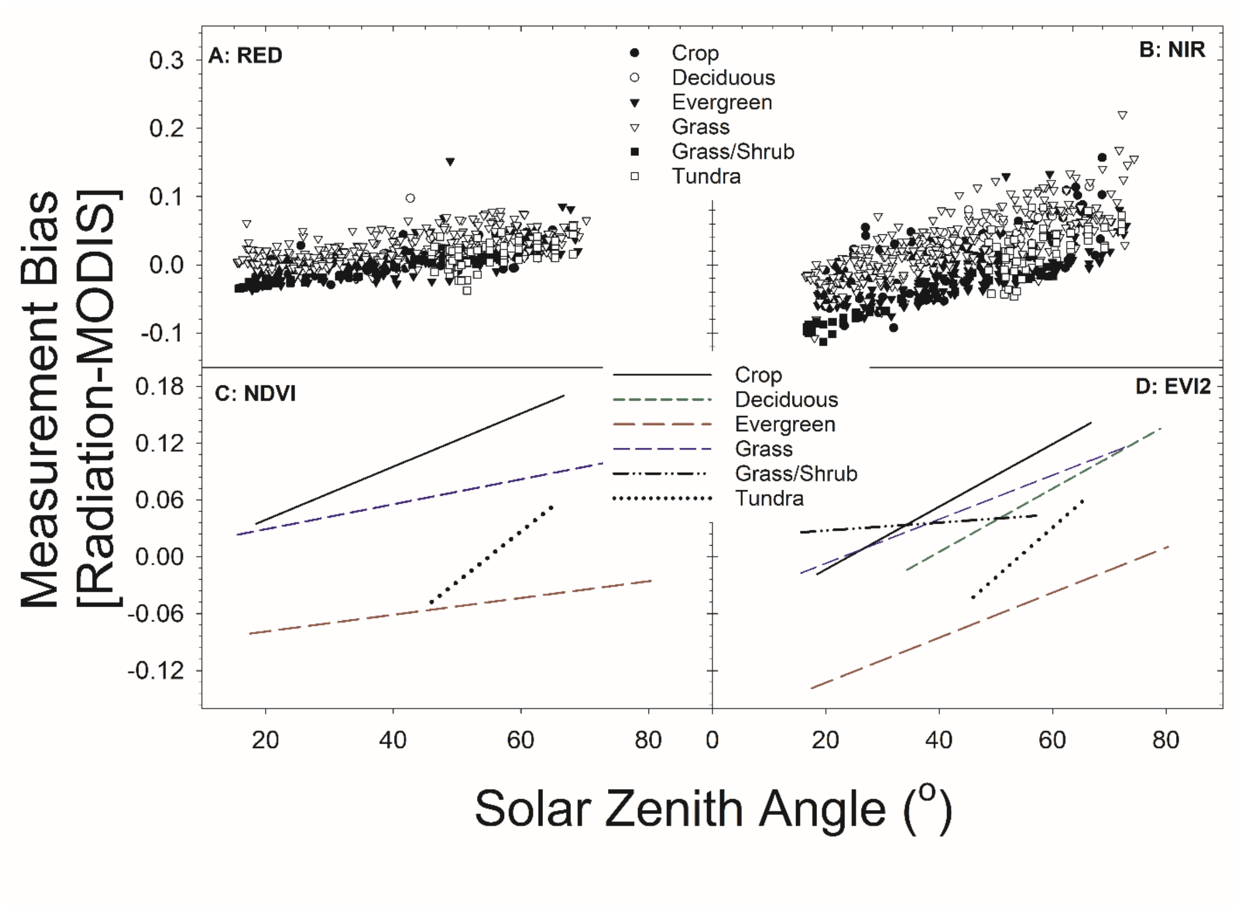
A: RED
B: NIR
C: NDVI
D: EVI2
Crop
Deciduous
Evergreen
Grass
Grass/Shrub
Tundra
Crop
Deciduous
Evergreen
Grass
Grass/Shrub
Tundra
0.3
0.2
0.1
0.0
-0.1
0.18
0.12
0.06
0.00
-0.06
-0.12
20
40
60
80
0
20
40
60
80
Measurement Bias
[Radiation-MODIS]
Solar Zenith Angle (o)

Figure 4.

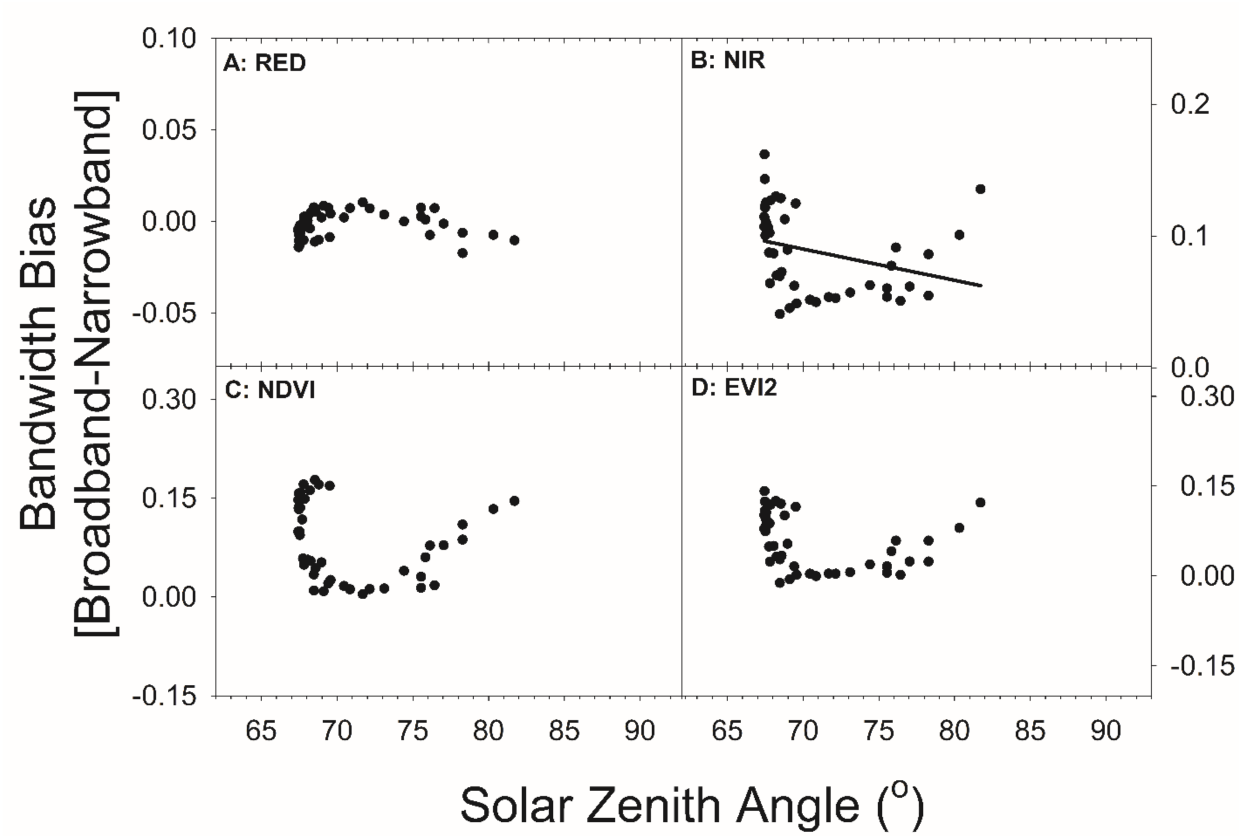
A: RED
B: NIR
C: NDVI
D: EVI2
Bandwidth Bias
[Broadband-Narrowband]
0.10
0.05
0.00
-0.05
0.30
0.15
0.00
-0.15
0.2
0.1
0.0
0.30
0.15
0.00
-0.15
65
70
75
80
85
90
Solar Zenith Angle (°)

Figure 5.

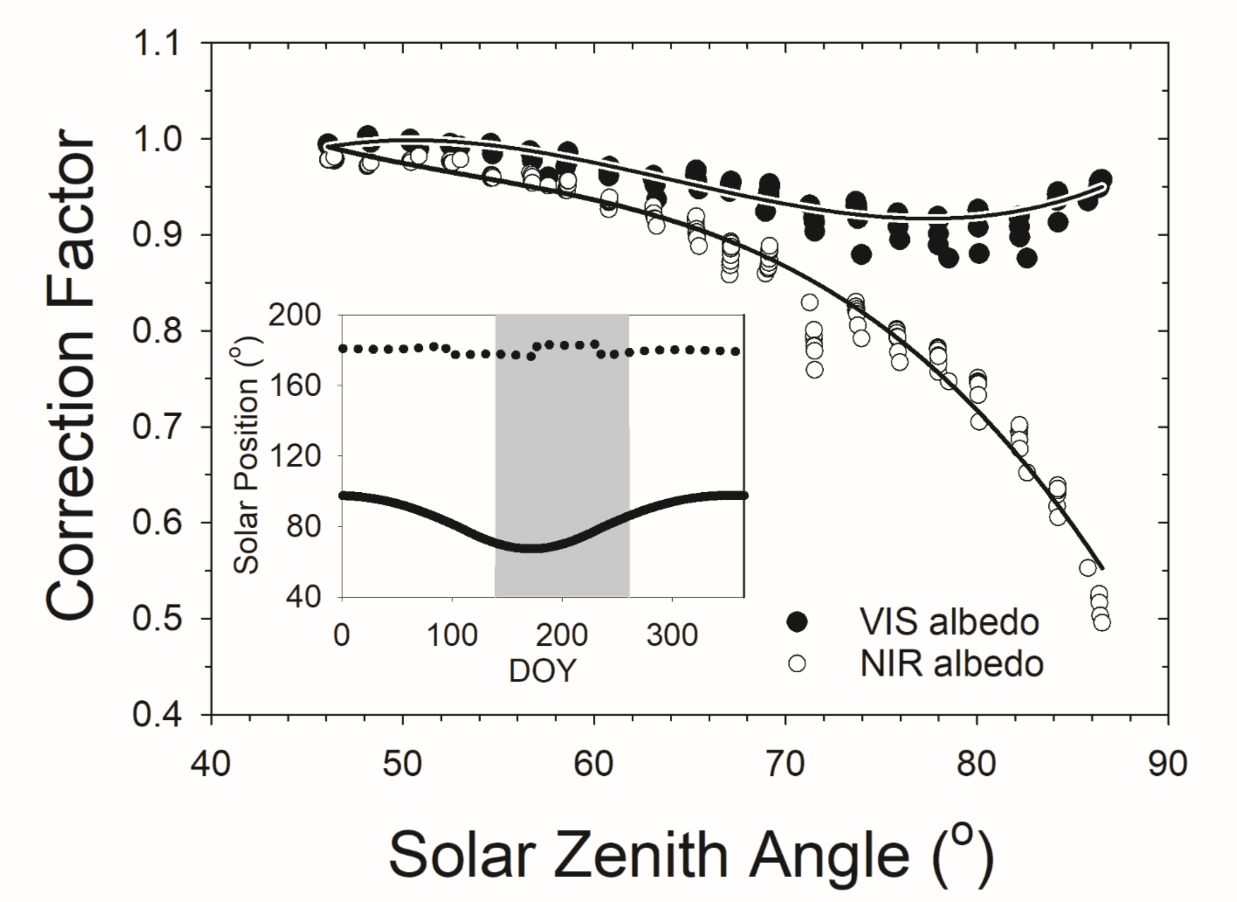

Correction Factor
1.1
1.0
0.9
0.8
0.7
0.6
0.5
0.4
40
50
60
70
80
90
Solar Zenith Angle (°)
Solar Position (°)
200
160
120
80
40
0
100
200
300
DOY
VIS albedo
NIR albedo

Figure 6.

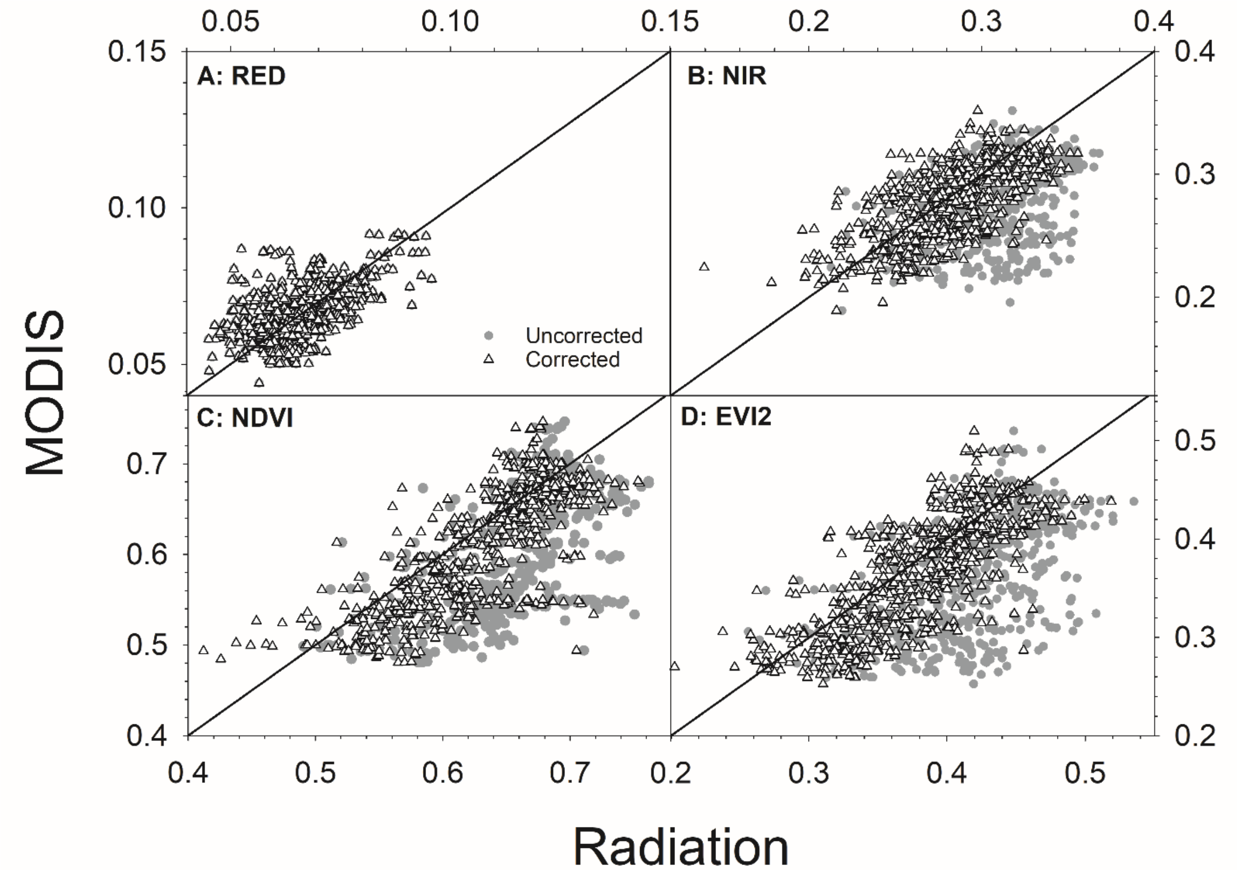

A: RED
B: NIR
C: NDVI
D: EVI2
Uncorrected
Corrected
MODIS
Radiation
0.05
0.10
0.15
0.2
0.3
0.4
0.5
0.6
0.7

Figure 7.

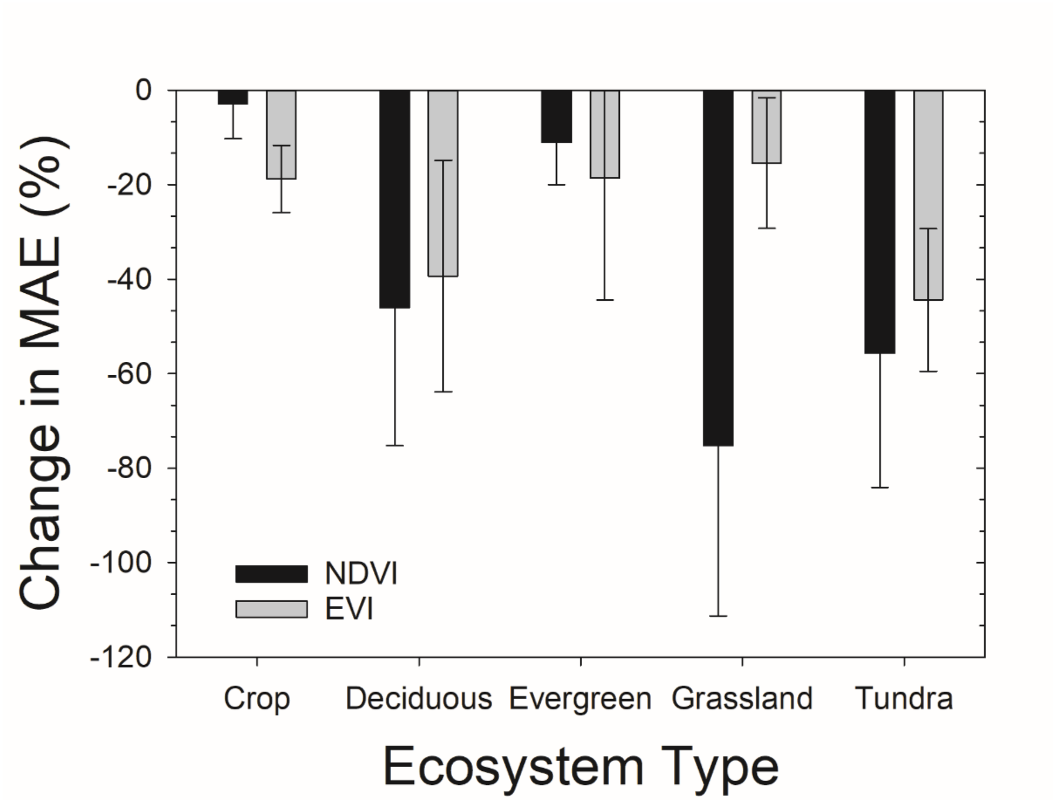
Change in MAE (%)
0
-20
-40
-60
-80
-100
-120
NDVI
EVI
Crop
Deciduous
Evergreen
Grassland
Tundra
Ecosystem Type

Figure 8.

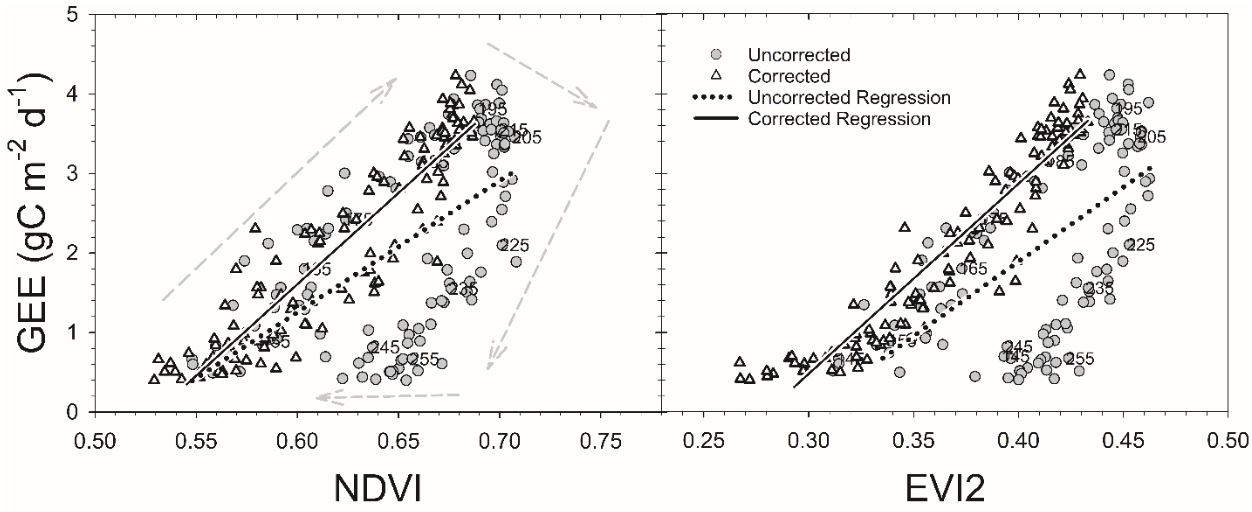
GEE (gC m-2 d-1)
NDVI
EVI2
Uncorrected
Corrected
Uncorrected Regression
Corrected Regression
195
205
225
235
245
255
165
0
1
2
3
4
5
0.50
0.55
0.60
0.65
0.70
0.75
0.25
0.30
0.35
0.40
0.45
0.50

Figure 9.

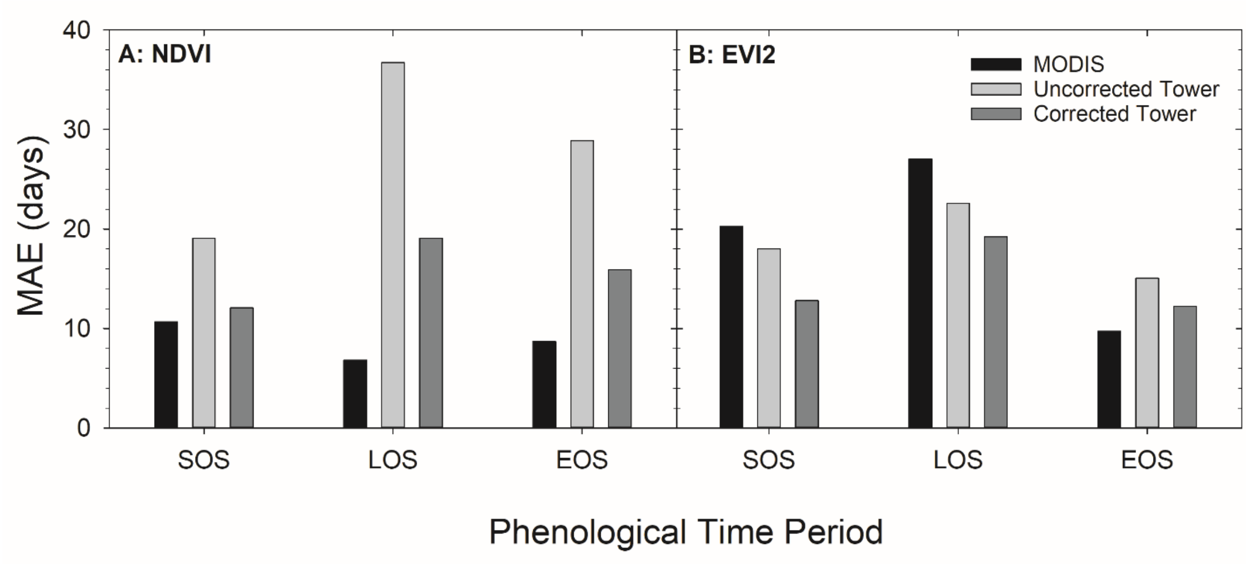

Figure 10.

Supplement:

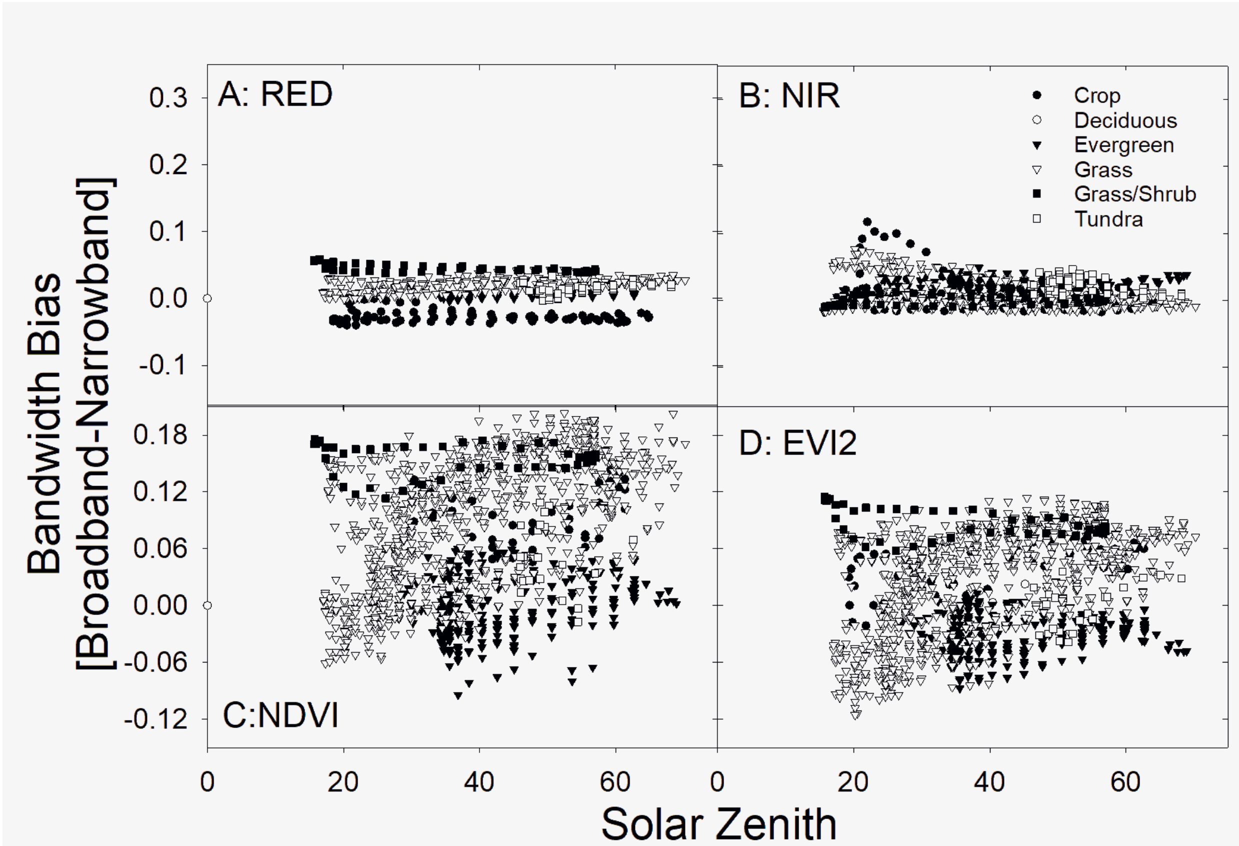

Figure 1S: Dependence of bandwidth biases (broadband-narrowband) derived differences on solar zenith angle for red reflectance (A), near infrared reflectance (B), NDVI (C), and EVI2 (D) from Fluxnet sites across biome types. Note that the y-axes are scaled to be the same as those observed in Figure 4.

Table 1S: Summary statistics for bandwidth bias correlation with solar zenith angle in Figure 1S. The number represents the R^2 of the relationship, while the number in [brackets] represents the sensitivity to solar zenith angle measured as the slope of the line.

PFT	Red (R^2 [Slope])	NIR (R^2 [Slope])	NDVI (R^2 [Slope])	EVI2 (R^2 [Slope])
Crop	**0.06 [-0.0001]**	**0.09 [-0.0005]**	0.01 [0.0002]	**0.37 [-0.0007]**
Deciduous	**0.46 [-0.0003]**	**0.14 [-0.0006]**	0.03 [0.0003]	**0.52 [-0.0046]**
Evergreen	**0.06 [0.0001]**	**0.12 [0.0003]**	**0.06 [0.00093]**	0.02 [0.0003]
Grass	**0.62 [0.0002]**	**0.11 [-0.0006]**	**0.06 [0.0009]**	**0.29 [0.002]**
Grass/Shrub	**0.10 [0.0001]**	**0.08 [-0.0005]**	0.01 [0.00003]	**0.22 [-0.0005]**
Tundra	**0.16 [0.0005]**	**0.22 [-0.0008]**	0.01 [-0.0001]	**0.29 [0.002]**

*Numbers in bold represent statistically significant relationships at the 95% Confidence level.

References:

Baldocchi, D.D. (2003). Assessing the eddy covariance technique for evaluating carbon dioxide exchange rates of ecosystems: past, present and future. *Global Change Biology, 9*, 479-492

Balzarolo, M., Anderson, K., Nichol, C., Rossini, M., Vescovo, L., Arriga, N., Wohlfahrt, G., Calvet, J.-C., Carrara, A., Cerasoli, S., Cogliati, S., Daumard, F., Eklundh, L., Elbers, J.A., Evrendilek, F., Handcock, R.N., Kaduk, J., Klumpp, K., Longdoz, B., Matteucci, G., Meroni, M., Montagnani, L., Ourcival, J.-M., Sánchez-Cañete, E.P., Pontailler, J.-Y., Juszczak, R., Scholes, B., & Martín, M.P. (2011). Ground-based optical measurements at European flux sites: a review of methods, instruments and current controversies. *Sensors (Basel, Switzerland), 11*, 7954-7981

Beck, P.S.A., Atzberger, C., Høgda, K.A., Johansen, B., & Skidmore, A.K. (2006). Improved monitoring of vegetation dynamics at very high latitudes: A new method using MODIS NDVI. *Remote Sensing of Environment, 100*, 321-334

Bhandari, S., Phinn, S., & Gill, T. (2011). Assessing viewing and illumination geometry effects on the MODIS vegetation index (MOD13Q1) time series: implications for monitoring phenology and disturbances in forest communities in Queensland, Australia. *International Journal of Remote Sensing, 32*, 7513-7538

Blonquist, J.M., Tanner, B.D., & Bugbee, B. (2009). Evaluation of measurement accuracy and comparison of two new and three traditional net radiometers. *Agricultural and Forest Meteorology, 149*, 1709-1721

Carroll, J.J., & Fitch, B.W. (1981). Effects of solar elevation and cloudiness on snow albedo at the South Pole. *Journal of Geophysical Research: Oceans, 86*, 5271-5276

Dore, S., Montes-Helu, M., Hart, S.C., Hungate, B.A., Koch, G.W., Moon, J.B., Finkral, A.J., & Kolb, T.E. (2012). Recovery of ponderosa pine ecosystem carbon and water fluxes from thinning and stand-replacing fire. *Global Change Biology, 18*, 3171-3185

Disney, M., Lewis, P., Thackrah, G., Quaife, T., & Barnsley, M. (2004). Comparison of MODIS broadband albedo over an agricultural site with ground measurements and values derived from Earth observation data at a range of spatial scales. *International Journal of Remote Sensing, 25*, 5297-5317

Elvidge, C.D., and Z. Chen. (1995). Comparison of broad-band and narrow-band red and near-infrared vegetation indices. Remote Sensing of Environment, 54:38-45.

Euskirchen, E.S., Bret-Harte, M.S., Scott, G.J., Edgar, C., & Shaver, G.R. (2012). Seasonal patterns of carbon dioxide and water fluxes in three representative tundra ecosystems in northern Alaska. *Ecosphere, 3*, art4

Euskirchen, E.S., Bret-Harte, M.S., Shaver, G.R., Edgar, C.W., & Romanovsky, V.E. (2017). Long-Term Release of Carbon Dioxide from Arctic Tundra Ecosystems in Alaska. *Ecosystems, 20*, 960-974

Fisher, J.I., Mustard, J.F., & Vadeboncoeur, M.A. (2006). Green leaf phenology at Landsat resolution: Scaling from the field to the satellite. *Remote Sensing of Environment, 100*, 265-279

Fisher, J.I., Richardson, A.D., & Mustard, J.F. (2007). Phenology model from surface meteorology does not capture satellite-based greenup estimations. *Global Change Biology, 13*, 707-721

Gamon, J.A., Coburn, C., Flanagan, L.B., Huemmrich, K.F., Kiddle, C., Sanchez-Azofeifa, G.A., Thayer, D.R., Vescovo, L., Gianelle, D., Sims, D.A., Rahman, A.F., & Pastorello, G.Z. (2010). SpecNet revisited: bridging flux and remote sensing communities. *Canadian Journal of Remote Sensing, 36*, S376-S390

Gamon, J.A., Rahman, A.F., Dungan, J.L., Schildhauer, M., & Huemmrich, K.F. (2006). Spectral Network (SpecNet)—What is it and why do we need it? *Remote Sensing of Environment, 103*, 227-235

Huemmrich, K.F., T.A. Black, P.G. Jarvis, J.H. McCaughey, F.G. Hall (1999). High temporal resolution NDVI phenology from micrometeorological radiation sensors. *Journal of Geophysical Research: Atmospheres, 104*, 27935-27944

Goulden, M.L., Winston, G.C., McMillan, A.M.S., Litvak, M.E., Read, E.L., Rocha, A.V., & Rob Elliot, J. (2006). An eddy covariance mesonet to measure the effect of forest age on land–atmosphere exchange. *Global Change Biology, 12*, 2146-2162

Hollinger, S.E., Beth, C., Reinke, and R.A. Peppler (1994). Illinois Climate Network: Site Descriptions, Instrumentation, and Data Management In C. Illinois State Water Survey, IL (Ed.) (p. 62)

Huete, A.R. (1987). Soil and Sun angle interactions on partial canopy spectra. *International Journal of Remote Sensing, 8*, 1307-1317

Jenkins, J.P., Richardson, A., Braswell, B., Ollinger, S.V., Hollinger, D., & Smith, M.-L. (2007). Refining Light-Use Efficiency Calculations for a Deciduous Forest Canopy Using Simultaneous Tower-Based Carbon Flux and Radiometric Measurements. *Agricultural and Forest Meteorology, 143*, 64-79

Jiang, Z., Huete, A., Didan, K., & Miura, T. (2008). *Development of a two-band enhanced vegetation index without a blue band*.

Kratzenberg, M.G., Beyer, H.G., Colle, S., & Albertazzi, A. (2006). Uncertainty Calculations in Pyranometer Measurements and Application, 689-698

Kriebel, K.T. (1979). Albedo of vegetated surfaces: its variability with differing irradiances. *Remote Sensing of Environment, 8*, 283-290

Liang, S. (2000). Narrowband to broadband conversions of land surface albedo I Algorithms. *Remote Sensing of Environment*, 76, 213-238.

Ma, X., Huete, A., & Tran, N.N. (2019). Interaction of Seasonal Sun-Angle and Savanna Phenology Observed and Modelled using MODIS. *Remote Sensing, 11*

McEwing, K.R., Fisher, J.P., & Zona, D. (2015). Environmental and vegetation controls on the spatial variability of CH4 emission from wet-sedge and tussock tundra ecosystems in the Arctic. *Plant and Soil, 388*, 37-52

Middleton, E.M. (1992). Quantifying reflectance anisotropy of photosynthetically active radiation in grasslands. *Journal of Geophysical Research: Atmospheres, 97*, 18935-18946

Myers, D.R. (2017). *Solar radiation: Practical modeling for renewable energy applications*. Boca Raton: CRC Press, https://doi.org/10.1201/b13898

ORNL DAAC (2018). MODIS and VIIRS Land Products Global Subsetting and Visualization Tool. ORNL DAAC, Oak Ridge, Tennesee, USA. Accessed: 12/31/2018. Subset obtained for Imnaviat product at 68.61° N; 149.31° W. time period: 1/1/2000 to 9/31/2018, subset size: variable. https://doi.org/10.3334/ORNLDAAC/1379.

Rahman, H., Verstraete, M.M., & Pinty, B. (1993). Coupled surface-atmosphere reflectance (CSAR) model: 1. Model description and inversion on synthetic data. *Journal of Geophysical Research: Atmospheres, 98*, 20779-20789

Ramsey, F.L.S., D.W. (2013). The statistical sleuth: A course in methods of data analysis. *Boston: Brooks/Cole, Cengage*

Richardson, A.D., Mahecha, M.D., Falge, E., Kattge, J., Moffat, A.M., Papale, D., Reichstein, M., Stauch, V.J., Braswell, B.H., Churkina, G., Kruijt, B., & Hollinger, D.Y. (2008). Statistical properties of random CO2 flux measurement uncertainty inferred from model residuals. *Agricultural and Forest Meteorology, 148*, 38-50

Rocha, A.V., & Shaver, G.R. (2009). Advantages of a two band EVI calculated from solar and photosynthetically active radiation fluxes. *Agricultural and Forest Meteorology, 149*, 1560-1563

Rocha, A.V., & Shaver, G.R. (2011). Burn severity influences postfire CO_2 exchange in arctic tundra. *Ecological Applications, 21*, 477-489

Ross, J., & Sulev, M. (2000). Sources of errors in measurements of PAR. *Agricultural and Forest Meteorology, 100*, 103-125

Rouse, J.W., Jr., R.H. Haas, D.W. Deering, J.A. Schell, and J.C. Haran (1974). Monitoring the vernal advancement and retrogradation (Green Wave Effect) of Natural Vegetation [Great Plains Cooridor]. *Earth Resources and Remote Sensing*

Schaaf, C.B., Gao, F., Strahler, A.H., Lucht, W., Li, X., Tsang, T., Strugnell, N.C., Zhang, X., Jin, Y., Muller, J.-P., Lewis, P., Barnsley, M., Hobson, P., Disney, M., Roberts, G., Dunderdale, M., Doll, C., d'Entremont, R.P., Hu, B., Liang, S., Privette, J.L., & Roy, D. (2002). First operational BRDF, albedo nadir reflectance products from MODIS. *Remote Sensing of Environment, 83*, 135-148

Schaepman-Strub, G., Schaepman, M.E., Painter, T.H., Dangel, S., & Martonchik, J.V. (2006). Reflectance quantities in optical remote sensing—definitions and case studies. *Remote Sensing of Environment, 103*, 27-42

Schmid, H.P. (1997). Experimental design for flux measurements: matching scales of observations and fluxes. *Agricultural and Forest Meteorology, 87*, 179-200

Scott, R.L., Hamerlynck, E.P., Jenerette, G.D., Moran, M.S., & Barron-Gafford, G.A. (2010). Carbon dioxide exchange in a semidesert grassland through drought-induced vegetation change. *Journal of Geophysical Research: Biogeosciences, 115*

Shuai, Y., Schaaf, C., Zhang, X., Strahler, A., Roy, D., Morisette, J., Wang, Z., Nightingale, J., Nickeson, J., Richardson, A.D., Xie, D., Wang, J., Li, X., Strabala, K., & Davies, J.E. (2013). Daily MODIS 500 m reflectance anisotropy direct broadcast (DB) products for monitoring vegetation phenology dynamics. *International Journal of Remote Sensing, 34*, 5997-6016

Sims, D.A., Rahman, A.F., Cordova, V.D., El-Masri, B.Z., Baldocchi, D.D., Flanagan, L.B., Goldstein, A.H., Hollinger, D.Y., Misson, L., Monson, R.K., Oechel, W.C., Schmid, H.P., Wofsy, S.C., & Xu, L. (2006). On the use of MODIS EVI to assess gross primary productivity of North American ecosystems. *Journal of Geophysical Research: Biogeosciences, 111*

Sims, D.A., Rahman, A.F., Vermote, E.F., & Jiang, Z. (2011). Seasonal and inter-annual variation in view angle effects on MODIS vegetation indices at three forest sites. *Remote Sensing of Environment, 115*, 3112-3120

Stoy, P.a.D., MC and Richardson, AD and Vargas, R and Barr, AG and Anderson, RS and Arain, MA and Baker, IT and Black, TA and Chen, JM and Cook, RB and Gough, CM and Grant, RF and Hollinger, DY and Izaurralde, RC and Kucharik, CJ and Lafleur, P and Law, BE and Liu, S and Lokupitiya, E and Luo, Y and Munger, JW and Peng, C and Poulter, B and Price, DT and Ricciuto, DM and Riley, WJ and Sahoo, AK and Schaefer, K and Schwalm, CR and Tian, H and Verbeeck, Hans and Weng, E (2013). Evaluating the agreement between measurements and models of net ecosystem exchange at different times and timescales using wavelet coherence: an example using data from the North American Carbon Program Site-Level Interim Synthesis. *Biogeosciences, 10*, 6893-6909

Tittebrand, A., U. Spank, C.H. Bernhofer (2009). Comparison of satellite- and ground-based NDVI above different land-use types. *Theoretical and Applied Climatology, 98*, 171-186

Ueyama, M., Iwata, H., Harazono, Y., Euskirchen, E.S., Oechel, W.C., & Zona, D. (2013). Growing season and spatial variations of carbon fluxes of Arctic and boreal ecosystems in Alaska (USA). *Ecological Applications, 23*, 1798-1816

Verma, S.B., Dobermann, A., Cassman, K.G., Walters, D.T., Knops, J.M., Arkebauer, T.J., Suyker, A.E., Burba, G.G., Amos, B., Yang, H., Ginting, D., Hubbard, K.G., Gitelson, A.A., & Walter-Shea, E.A. (2005). Annual carbon dioxide exchange in irrigated and rainfed maize-based agroecosystems. *Agricultural and Forest Meteorology, 131*, 77-96

Wang, Q., Tenhunen, J., Dinh, N.Q., Reichstein, M., Vesala, T., & Keronen, P. (2004). Similarities in ground- and satellite-based NDVI time series and their relationship to physiological activity of a Scots pine forest in Finland. *Remote Sensing of Environment, 93*, 225-237

Wang, X., & Zender, C.S. (2010). Constraining MODIS snow albedo at large solar zenith angles: Implications for the surface energy budget in Greenland. *Journal of Geophysical Research: Earth Surface, 115*

Wang, Z., Barlage, M., Zeng, X., Dickinson, R.E., & Schaaf, C.B. (2005). The solar zenith angle dependence of desert albedo. *Geophysical Research Letters, 32*

Wang, Z., Schaaf, C.B., Chopping, M.J., Strahler, A.H., Wang, J., Román, M.O., Rocha, A.V., Woodcock, C.E., & Shuai, Y. (2012). Evaluation of Moderate-resolution Imaging Spectroradiometer (MODIS) snow albedo product (MCD43A) over tundra. *Remote Sensing of Environment, 117*, 264-280

Wilson, T.B., & Meyers, T.P. (2007). Determining vegetation indices from solar and photosynthetically active radiation fluxes. *Agricultural and Forest Meteorology, 144*, 160-179

Wittich, K.-P., & Kraft, M. (2008). The normalised difference vegetation index obtained from agrometeorological standard radiation sensors: a comparison with ground-based multiband spectroradiometer measurements during the phenological development of an oat canopy. *International Journal of Biometeorology, 52*, 167-177

Wohlfahrt, G., Pilloni, S., Hörtnagl, L., & Hammerle, A. (2010). Estimating carbon dioxide fluxes from temperate mountain grasslands using broad-band vegetation indices. *Biogeosciences (Online), 7*, 683-694

Wright, K.S., & Rocha, A.V. (2018). A test of functional convergence in carbon fluxes from coupled C and N cycles in Arctic tundra. *Ecological Modelling, 383*, 31-40

Xiao, X., Zhang, Q., Hollinger, D., Aber, J., & Moore Iii, B. (2005). Modeling gross primary production of an evergreen needleleaf forest using MODIS and climate data. *Ecological Applications, 15*, 954-969

Xiong, X., N. Che, W.L. Barnes. (2006). Terra MODIS On-orbit spectral characterization and performance. IEEE Transactions on Geoscience and Remote Sensing. 44(8): 2198-2206.

Yang, F., Mitchell, K., Hou, Y.-T., Dai, Y., Zeng, X., Wang, Z., & Liang, X.-Z. (2008). Dependence of Land Surface Albedo on Solar Zenith Angle: Observations and Model Parameterization. *Journal of Applied Meteorology and Climatology, 47*, 2963-2982

Zhao, D., L. Huang, J. Li, J. Qi. (2007) A comparative analysis of broadband and narrowband derived vegetation indices in predicting LAI and CCD of a cotton canopy. *Journal of Photogrammetry & Remote Sensing*, 62, 25-33.